

# The CI lines as tracers of molecular gas, and their prospects at high redshifts

P. P. Papadopoulos,<sup>1,2</sup> W.-F. Thi,<sup>3</sup> and S. Viti,<sup>1,4</sup>

<sup>1</sup>*Department of Physics & Astronomy, University College London, London, WC1E 6BT, UK*

<sup>2</sup>*ESA Astrophysics Division, Research and Scientific Support Department, ESTEC, Postbus 299, 2200 AG Noordwijk, The Netherlands*

<sup>3</sup>*Sterrenkundig Instituut “Anton Pannekoek”, Kruislaan 403, 1098 SJ Amsterdam, The Netherlands*

<sup>4</sup>*CNR-Istituto di Fisica dello Spazio Interplanetario, Area di Ricerca di Tor Vergata, via del fosso del Cavaliere 100, 00133, Roma, Italy*

Received; Accepted

## ABSTRACT

We examine the fine structure lines  $^3P_1 \rightarrow ^3P_0$  (492 GHz) and  $^3P_2 \rightarrow ^3P_1$  (809 GHz) of neutral atomic carbon as bulk molecular gas mass tracers and find that they can be good and on many occasions better than  $^{12}\text{CO}$  transitions, especially at high redshifts. The notion of CI emission as an  $\text{H}_2$  gas mass tracer challenges the long-held view of its distribution over only a relatively narrow layer in the CII/CI/CO transition zone in FUV-illuminated molecular clouds. Past observations have indeed consistently pointed towards a more extended CI distribution but it was only recently, with the advent of large scale imaging of its  $^3P_1 \rightarrow ^3P_0$  transition, that its surprising ubiquity in molecular clouds has been fully revealed. In the present work we show that under *typical* ISM conditions such an ubiquity is inevitable because of well known dynamic and non-equilibrium chemistry processes maintaining a significant  $[\text{C}]/[^{12}\text{CO}]$  abundance throughout Giant Molecular Clouds during their lifetime. These processes are more intense in star-forming environments where a larger ambient cosmic ray flux will also play an important role in boosting  $[\text{C}]/[^{12}\text{CO}]$ . The resulting CI lines can be bright and effective  $\text{H}_2$  mass tracers especially for diffuse ( $\sim 10^2 - 10^3 \text{ cm}^{-3}$ ) gas while in UV-intense and/or metal-poor environments their  $\text{H}_2$ -tracing capability diminishes because of large scale CII production but nevertheless remains superior to that of  $^{12}\text{CO}$ . The best place to take full advantage of CI’s capacity to trace  $\text{H}_2$

is not in the low- $z$  Universe, where large atmospheric absorption at 492 and 809 GHz precludes routine observations, but at high redshifts ( $z \gtrsim 1$ ).

**Key words:** Galaxies – starburst – galaxies: sub-mm – galaxies: Ly-break – ISM: molecules – ISM: abundances – ISM: atoms

## 1 INTRODUCTION

The use of  $^{12}\text{CO}$  and its isotopologues rotational lines to measure  $\text{H}_2$  gas mass and physical properties in galaxies is now a well-established technique (e.g. Dickman et al. 1986; Elmegreen 1989; Bryant & Scoville 1996) employed successfully throughout the local Universe ( $z \lesssim 0.3$ ) (e.g. Sanders, Scoville & Soifer 1991; Young & Scoville 1991; Solomon et al. 1992; Downes & Solomon 1998) and at increasingly high redshifts (e.g. Brown & Vanden Bout 1991; Downes et al. 1992; Omont et al. 1996; Frayer et al. 1998). In high- $z$  observations usually only high- $J$  CO lines  $J + 1 \rightarrow J$ , ( $J + 1 \geq 4$ ) are accessible for evaluating the mass and physical conditions of  $\text{H}_2$  gas, thus omitting cooler ( $T_{\text{kin}} < 30$  K) and/or sub-thermally excited gas ( $n < 10^4 \text{ cm}^{-3}$ ). Recently observations of the lowest  $^{12}\text{CO}$   $J=1-0$ ,  $2-1$  transitions in several high redshift objects have been made possible with the Very Large Array (e.g. Carilli, Menten, & Yun 1999; Carilli et al. 2002a, 2002b) and in some cases thermalized transitions up to fairly high rotational levels (e.g.  $J=5-4$ ) have been observed. However, differential lensing can complicate standard interpretation of line ratios by preferentially amplifying the emission of the usually more spatially confined warm and dense gas (e.g. Blain 1999) yielding the false impression that such gas properties (and the thermalization of high- $J$  CO transitions) characterize the bulk of the molecular gas in such systems. In one case of an unlensed high- $z$  starburst large scale sub-thermal excitation of  $^{12}\text{CO}$   $J=5-4$  has been inferred (Papadopoulos & Ivison 2002).

Another limitation of the standard method is encountered in tracing metal-poor  $\text{H}_2$  gas, which becomes more severe in enhanced FUV radiation fields: the reduced dust-shielding and CO self-shielding allows UV photons to dissociate CO while leaving the mostly self-shielding  $\text{H}_2$  intact (Maloney & Black 1988; Israel 1988, 1997). This is now corroborated by observations of the metal-poor outer parts of typical spirals (Nakai & Kuno 1995; Arimoto, Sofue, & Tsujimoto 1996), globally metal-poor objects like the Magellanic Clouds and Magellanic Irregulars (e.g. Madden et al. 1997), and blue compact dwarf galaxies (e.g. Barone et al. 2000). Unfortunately both types of the aforementioned bias can hinder efforts to measure  $\text{H}_2$

gas mass at high redshifts since high- $J$   $^{12}\text{CO}$  lines are those used most often, and significant amounts of metal-poor gas reside in UV-intense environments (e.g. in Ly-break galaxies).

The CI J=1–0 line was one of the first Photodissociation Region (PDR) lines to be detected from molecular clouds (Phillips & Huggins 1981), yet its  $H_2$  tracing potential has gone unnoticed. There are three main reasons for that namely, a) the low atmospheric transmission at its rest-frame frequency of  $\sim 492$  GHz precluded, until recently, routine observations of molecular clouds in this transition, b) instrumentation constraints in terms of receiver sensitivity and the ability to map large areas fast (no multi-beam receivers available), and c) an early theoretical prejudice of one-dimensional steady-state PDR models that pictured CI distributed only in a relatively narrow CII/CI/CO transition zone on the surface of FUV-illuminated molecular clouds (e.g. Tielens & Hollenbach 1985a,b) and thus unable to trace the bulk of their mass. Interestingly this prejudice was at times reinforced by the instrumentation and atmospheric restrictions which allowed only limited mapping of CI emission, which in turn was mainly conducted in regions where theory predicted CI should be. These early views on the CI distribution in PDRs could explain some general features of its emission such as the surprising robustness of the CI J=1–0 line brightness over a wide range of FUV intensities and metallicities (e.g. Kaufman 1999).

This simple picture is now challenged by two large scale CI surveys of the Orion A and B molecular clouds (Ikeda et al. 2002) and the Galactic Center (Ojha et al. 2001) that find CI,  $^{12}\text{CO}$ , and  $^{13}\text{CO}$  J=1–0 emission to be fully co-extensive, their intensities tightly correlated, and with a surprisingly constant  $N(\text{CI})/N(^{12}\text{CO}) \sim 0.1 - 0.2$  ratio over dramatic changes in ambient FUV field and physical conditions. These observations along with a considerable body of similar past observational evidence (see Keene 1997 for a review) point to a CI distribution fully concomitant with that of CO. The present work uses time-varying chemical models under typical conditions found in Giant Molecular Clouds (GMCs) to further elucidate this issue, and then examines the potential of CI line emission as an  $H_2$  mass tracer. We focus mainly on the following issues,

- 1) The current state of the art of CI observations revealing its distribution throughout molecular clouds (thus allowing it to be a tracer of their mass), and the role of non-equilibrium and/or dynamic processes as well as cosmic rays under typical ISM conditions.
- 2) The expected CI line flux densities over a range of physical conditions and their relative observational advantage (if any) with respect to the  $^{12}\text{CO}$  transitions.
- 3) The uncertainties of  $H_2$  mass estimates from CI emission with respect to those associated

with the standard method employing CO lines, as well as the observational prospects of using the CI lines to trace molecular gas at high redshifts.

Throughout this work, we adopt a  $q_0 = 0.5$  cosmology with  $\Omega_\Lambda = 0$ .

## 2 THE DISTRIBUTION OF CI IN GMCS

In an early attempt to account for the mounting number of observations finding CI to be more extended than predicted by the models (e.g. Keene et al. 1985) low density PDRs ( $n \sim 100 \text{ cm}^{-3}$ ) have been advocated. There the CI abundance in the CII/CI/CO transition zone becomes larger ( $[\text{C}]/[^{12}\text{CO}] \sim 1 - 100$ ) than in denser ones ( $n \geq 10^4 \text{ cm}^{-3}$ ) because a different, CI-rich, chemical route is favored, allowing CI to dominate over a larger region of the cloud,  $A_v \sim 3-7$  (Hollenbach, Takahashi, & Tielens 1991). More realistic inhomogeneous PDR models showed a deeper FUV penetration and a more pervasive CI emission “coating” the clumps making up the GMCs (Meixner & Tielens 1993; Spaans & van Dishoeck 1997).

The aforementioned schemes can produce a *spatial* correlation between CI emission and that of  $\text{H}_2$  mass tracers like the  $^{12}\text{CO}$ ,  $^{13}\text{CO}$  J=2–1, 1–0 transitions but cannot readily explain their tight *intensity* correlation (Keene et al. 1997). The latter is surprising because e.g. a CI/ $^{13}\text{CO}$  intensity ratio should depend on quantities like the surface-layer to total cloud mass ratio, the different ambient excitation conditions of the two species (even in clumped PDRs CI and  $^{13}\text{CO}$  still reside in different volumes), all expected to vary strongly within a molecular cloud and between clouds. The discovery of significant CI emission deep in UV-protected sites of cold dark clouds in the Galaxy (e.g. Oka et al. 2001), and M 31 (Israel, Tilanus, & Baas 1998) makes the standard steady-state PDR interpretation (with typical cosmic ray fluxes) even more difficult. In the few cases where CI J=2–1 is also detected, the CI (2–1)/(1–0) ratio yields (in LTE) similar gas temperatures to those deduced solely from the  $^{12}\text{CO}$  lines or FIR/sub-mm dust continuum in either starburst or quiescent environments (Stutzki et al. 1997 and references therein). Finally the striking similarity of CI and  $^{13}\text{CO}$  line profiles in the latest large scale survey by Ikeda et al. (2002) suggests a spatial and intensity correlation continuing to still smaller scales than those probed by the nominal resolution of the particular observations of  $\sim 0.3 \text{ pc}$  (assuming macroscopic motions of much smaller, radiatively-decoupled “cells” responsible for line-formation in GMCs, see e.g. Tauber 1996). *The simplest explanation of all the aforementioned observational results is that CI and CO are fully concomitant and trace the same  $\text{H}_2$  gas mass.*

## 2.1 Is the [C]/[CO] equilibrium reachable?

Non-equilibrium chemical processes can maintain a high [CI]/[ $^{12}\text{CO}$ ] in cloud regions that have not attained chemical equilibrium (e.g. de Boisanger & Chiéze 1991; Lee et al. 1996; Störzer, Stutzki, & Sternberg 1997), or have done so under turbulent diffusive “mixing” of a CI-rich cloud envelope with its deeper regions (Xie, Allen, & Langer 1995; Xie 1997). The most recent investigation of the time dependence of the [C]/[ $^{12}\text{CO}$ ] ratio and the resulting CI line intensities by Störzer et al. examines the effects of abrupt changes of a strong local FUV field intensity ( $G_\odot \sim 10^5$ ) caused by cloud-cloud shadowing over timescales of  $\lesssim 10^5$  yrs.

In the present work we assume ambient conditions expected for the bulk of the molecular gas in GMCs rather than in their few O, B star-illuminated hot/dense spots. These conditions consists of: a) initially atomic clouds (the likely precursors of GMCs), b) softer ambient FUV fields, and c) a larger range of gas densities. Moreover, processes other than cloud-cloud shadowing govern the evolution of GMCs and their ambient conditions, with timescales short enough to allow them to maintain a high [C]/[ $^{12}\text{CO}$ ] ratio throughout the volume of a typical GMC during its lifetime.

In the case of chemical processes the  $H_2$  formation timescale provides a good approximation for an overall equilibrium to be reached in a molecular cloud that is initially atomic (e.g. Hollenbach & Tielens 1999). This timescale is

$$t_{\text{ch}} \sim (2\langle n \rangle R_f)^{-1} = 10^7 \left( \frac{T}{100\text{K}} \right)^{-1/2} \left( \frac{\langle n \rangle}{50\text{cm}^{-3}} \right)^{-1} \text{ yrs}, \quad (1)$$

where  $\langle n \rangle$  is the average H density and  $R_f = 3 \times 10^{-18} (T/\text{K})^{1/2} \text{ cm}^3 \text{ s}^{-1}$  is the canonical  $H_2$  formation rate on dust grains (e.g. Jura 1975). For  $\langle n \rangle \sim (20-60) \text{ cm}^{-3}$  and  $T \sim (70-120) \text{ K}$  (typical for the Cold Neutral Medium HI out of which GMCs form), it is  $t_{\text{ch}} \sim (1-3) \times 10^7$  yrs.

On the other hand, the dynamic evolution timescale is

$$t_{\text{dyn}} = \left( \frac{3\pi}{16G\langle \rho \rangle} \right)^{1/2} \sim 0.9 \times 10^7 \left( \frac{\langle n \rangle}{50\text{cm}^{-3}} \right)^{-1/2} \text{ yrs}, \quad (2)$$

(spherical cloud assumed). This is comparable to  $t_{\text{ch}}$  and is in accordance with the well known fact that timescales of  $\sim (10^6 - 10^7)$  yrs characterize a wide variety of processes that fully disrupt or otherwise drastically alter typical GMCs. Some of the most important ones are star formation with the disruptive effects of O, B, star clusters (e.g. Bash, Green, & Peters 1977), turbulent dissipation (Stone, Ostriker, & Gammie 1998; MacLow et al. 1998), and inter-cloud clump-clump collisions (Blitz & Shu 1980). The fact that these timescales are shorter or comparable to  $t_{\text{ch}}$  suggests that molecular clouds may never reach chemical equilibrium.

Driven by the evolution of continuously forming stellar populations throughout a galaxy, the *average* FUV field regulating the CII/CI/CO transition zone in stationary PDR models also varies. Recent work by Parravano, Hollenbach & McKee (2003) has shown

$$t_{\text{FUV}} = k\lambda_{\text{SFR}}^{-1} \left( \frac{U}{U_{\odot}} \right)^{3/2} 10^6 \text{ yrs}, \quad (3)$$

to be the typical time needed for a significant perturbation of the FUV energy density to occur, where  $k = 1 - 2$ ,  $U$  is the FUV energy density,  $U_{\odot} = 10^{-17} \text{ ergs cm}^{-3} \text{ \AA}^{-1}$ , and  $\lambda_{\text{SFR}}$  is the star formation rate normalized to its Solar neighborhood value. For e.g.  $U = 10 \times U_{\odot}$  it is  $t_{\text{FUV}} \sim 5 \times 10^7 \text{ yrs}$ , comparable to  $t_{\text{ch}}$  even in quiescent environments ( $\lambda_{\text{SFR}} = 1$ ).

In order to track the evolution of the  $[\text{C}]/[^{12}\text{CO}]$  ratio during the aforementioned timescales we present results from our homogeneous, time-dependent PDR models in Figure 1. The chemistry of gas is represented over a semi-infinite slab, taking into account all the heating and cooling processes (see Papadopoulos, Thi, & Viti 2002 and references therein). We have also included the latest advancements in collisional/reaction rates and chemical networks which now include most charge-exchange reactions. The latter are particularly important in the proper estimate of the  $[\text{C}]/[^{12}\text{CO}]$  values in heavily shielded, cosmic ray-dominated environments with various metallicities (sections 2.2, 2.3).

The diagrams in Figure 1 confirm that the  $[\text{CI}]/[^{12}\text{CO}]$  equilibrium timescale and  $t_{\text{dyn}}$  (Equation 2) remain comparable throughout the density range examined. Hence, since self-gravity is the plausible main “driver” behind many processes altering the physical conditions of a GMC (e.g. star formation; Elmegreen 2002), it can be argued that  $[\text{CI}]/[^{12}\text{CO}]$  remains significant, never settling to its (small) equilibrium values throughout its lifetime. In more active star forming environments all processes that disrupt GMCs or alter their ambient conditions operate on still shorter timescales. The effect of higher star formation rates is easily highlighted by Equation 3 since for  $\lambda_{\text{SFR}} > 1$ ,  $t_{\text{FUV}}$  simply becomes proportionally shorter.

In the absence of a generally accepted GMC formation and destruction theory the most general way to view the effects of elevated star formation on chemical equilibrium is by assuming that star formation powers the cycling of interstellar gas between the Warm, Cold HI (WNM, CNM), and the molecular gas phases. Then the gas condensation rate  $\omega(n_{\text{H}}) = d(\log n_{\text{H}})/dt = \phi_{\text{SFR}}/g(n_{\text{H}})$ , where  $g(n_{\text{H}}) = \partial M/\partial(\log n_{\text{H}})$  is the mass fraction per logarithmic density interval (Liou & Chiéze 1990). Clearly, irrespective of the particular physical processes defining  $\omega(n_{\text{H}})$ , a higher  $\phi_{\text{SFR}}$  induces a faster evolution of any given gas

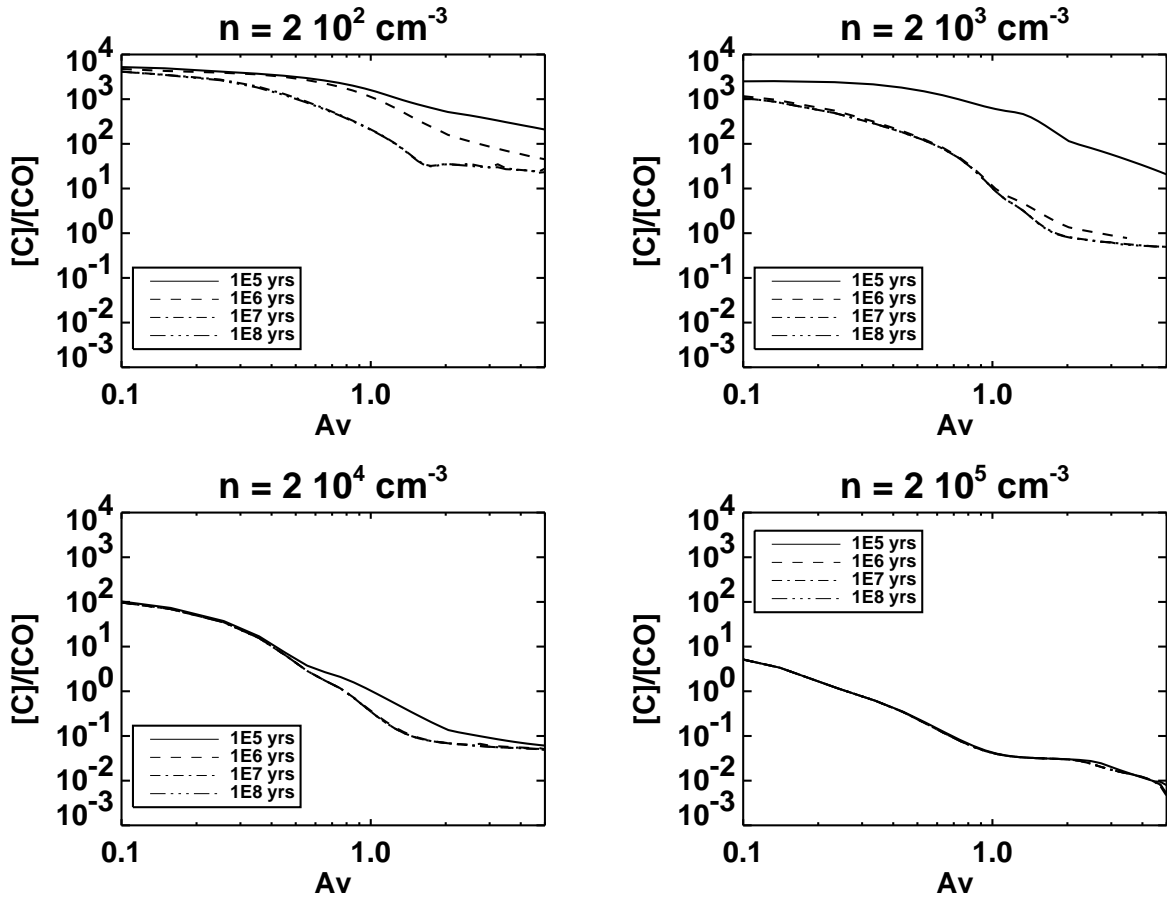


**Figure 1.** Results from a time-dependent PDR code (see text) for an initially atomic cloud with one-sided illumination by a unidirectional FUV field and densities shown at the top of each frame. The assumed metallicity is solar ( $Z=1$ ) and the incident radiation field is  $G_0 = 1/2$ , (corresponding to one-sided illumination by a Habing field). The well-known  $[C]/[^{12}CO]$  enhancement in low density gas with respect to denser gas is clearly discernible

“parcel” across the entire mass-density spectrum of the neutral ISM, leaving less time for it to reach chemical equilibrium at any one phase.

## 2.2 The role of turbulence

A relatively recent observational result that is particularly hard to reconcile with steady-state models was obtained by the extensive CI  $J=1-0$  and  $^{12}CO$   $J=4-3$  imaging of the Carina molecular clouds where a close spatial association of their emission throughout the cloud was found, suggesting that the same gas emits both lines (Zhang et al. 2001). Low density PDRs ( $\sim 10^2 \text{ cm}^{-3}$ ) would be CI-rich and bright in CI  $J=1-0$  but not in the  $^{12}CO$   $J=4-3$  transition that has  $n_{43} \sim 2 \times 10^4 \text{ cm}^{-3}$ , while in the bi-stability scenario (section 2.2) a locally much higher CR flux (so that  $n_{(CR)} \gtrsim 10^4 \text{ cm}^{-3}$ ) would be needed to explain such association.

Turbulent diffusion can smooth any initial  $[CI]/[^{12}CO]$  abundance gradient so that it becomes almost constant throughout a typical cloud, and in the Carinae molecular complex

the clouds are found to be warmer than typical ones in the disk, suggestive of turbulent velocity field dissipation (Zhang et al. 2001). The effects of turbulent diffusion on elemental abundances have been outlined by Xie, Allen, & Langer (1995) (see also Xie 1997 for a review), and here we will only point out the effects in the kinematically violent environments found in e.g. galactic centers and merger systems. In such regions molecular clouds have very high velocity dispersions, typically  $\sigma_V \sim 50 \text{ km s}^{-1}$  for the Galactic Center (e.g. Oka et al. 1996), that can reach up to  $\sim (50 - 100) \text{ km s}^{-1}$  in the extreme ULIRG merger systems (albeit model-dependent, e.g. Downes & Solomon 1998). These are much higher than  $\sim (1 - 5) \text{ km s}^{-1}$  found for GMCs in the kinematically quiescent spiral disks. These large line widths in kinematically violent environment correspond to a turbulent diffusion coefficient  $K = \langle V_t L \rangle \sim (10^{24} - 10^{25}) \text{ cm}^2 \text{ s}^{-1}$ , (assuming  $\sigma_V \sim V_t$  and an invariant characteristic length scale  $L$ ). This is 1-2 orders of magnitude larger than in kinematically quiescent environments and can easily yield a constant  $[C]/[^{12}\text{CO}] \sim 0.1 - 1$  ratio throughout the cloud (Xie et al. 1995). The diffusion timescales are short, e.g. for quiescent GMCs  $t_{\text{diff}} \sim 3 \times 10^6$  yrs, which is shortened to  $\sim 3 \times (10^4 - 10^5)$  yrs in dynamically active environments ( $t_{\text{diff}} \propto 1/K$ ).

Such effects, and a potentially large cosmic ray flux (section 2.3), can easily account for the significant  $[CI]/[^{12}\text{CO}]$  ratios found in dark and dense clouds, shielded from the ambient FUV radiation by very large extinctions (e.g. Ikeda et al. 2002), as well as the similarity of CI J=1-0 and HCO<sup>+</sup> J=1-0, 3-2, CS J=2-1 line profiles (Stark et al. 1997; Johansson et al. 1994). The latter are particularly puzzling since in shielded environments HCO<sup>+</sup> is a product of dense, dark cloud chemistry, and its J=3-2 transition has  $n_{\text{cr}} \sim 10^6 \text{ cm}^{-3}$  which, along with CS J=2-1 ( $n_{\text{cr}} \sim 10^5 \text{ cm}^{-3}$ ), imply very dense gas for which standard PDR models predict <sup>12</sup>CO to be the dominant carbon-bearing species ( $[CI]/[^{12}\text{CO}] < 10^{-3}$ ). Turbulence has the strength and the time to redistribute any CI-rich, PDR-origin gas phase initially located in a cloud envelope throughout its denser and UV-shielded interior within its lifetime.

### 2.3 Processes controlling $[CI]/[^{12}\text{CO}]$ : the role of cosmic rays

The previous brief exposition of time-dependent chemical and dynamic phenomena suggests that *except in few of their densest, most UV-protected and kinematically quiescent regions, GMCs may never attain chemical equilibrium while turbulence is capable of “mixing” the resulting CI-rich gas phase throughout their volume*, a situation accentuated in star forming and/or dynamically active environments.



In star forming environments the expected larger cosmic ray flux will also raise the  $[CI]/[^{12}CO]$  ratio deep inside a cloud's volume, and several observations have indeed found a systematically larger  $[CI]/[^{12}CO]$  ratio in starburst nuclei (e.g. Harrison et al. 1995; Israel & Baas 2002). In the starburst M 82, bright CI J=1–0 emission with  $N(CI)/N(^{12}CO) \sim 0.5$  is measured over the bulk of its  $H_2$  gas (Schilke et al. 1993; White et al. 1994) while the CR flux in its central regions is  $F_{CR} \sim (170 - 500) \times F_{CR}^{(Gal)}$  (Suchkov, Allen, & Heckman 1993).

In Figure 2 the effect of  $F_{CR}$  on the CI distribution is presented, and the CR-induced  $[CI]/[^{12}CO]$  enhancement throughout a cloud becomes apparent (see also Flower et al. 1994 for early such work). Indeed in the dark cloud conditions prevailing deep into the inner regions of GMCs a pure PDR origin of CI becomes unattainable but cosmic rays, unlike ultraviolet photons, penetrate deep into clouds and at high  $A_v$  control both thermal balance and chemistry. Such a chemistry can still yield a steady-state CI-rich gas phase, provided  $n \lesssim n_{(CR)}$ . This “turnover” density increases for higher  $F_{CR}$  and marks a CR-controlled bi-stability of the chemical network set by the abrupt transition between two possible ISM ionization states (des Forêts, Roueff, & Flower 1992; Le Bourlot, des Forêts, & Roueff 1993; Flower et al. 1994). For  $n \lesssim n_{(CR)}$  the gas has a high ionization fraction and thus a high  $H_3^+$  dissociative recombination, allowing  $H^+$  to be the dominant ion and initiate a set of chemical reactions that yield  $[CI]/[^{12}CO] \sim 0.1 - 0.2$ . For  $n > n_{(CR)}$ ,  $H_3^+$  becomes dominant and a different chemical network yields a much lower  $[C]/[^{12}CO] \lesssim 10^{-3}$ .

For the Galaxy it is  $n_{(CR)} \sim 5 \times 10^3 \text{ cm}^{-3}$  (Schilke et al. 1993 and references therein), encompassing a large fraction of the molecular gas in GMCs. For totally shielded environments ( $G_o = 0$ ) and  $F_{CR} = F_{CR}^{(Gal)}$  our models yield  $[C]/[^{12}CO] \gtrsim 3$  for  $n \leq 10^3 \text{ cm}^{-3}$ , and  $[C]/[^{12}CO] \leq 0.02$  for  $n \geq 5 \times 10^3 \text{ cm}^{-3}$ . A ten-fold increase in  $F_{CR}$  boosts the aforementioned densities by an order of magnitude, for similar  $[C]/[^{12}CO]$  values. These values are in good accordance with those reported in the literature even though controversies remain and a major benchmarking effort of the various PDR codes is under way. In an important recent development the canonical value of  $F_{CR}$  in quiescent diffuse clouds in the Solar neighborhood may have to be revised upwards by a factor of  $\sim 40$  (McCall et al. 2003) thus opening up the possibility of a mainly CR-origin of the CI emission observed to be widely distributed in the quiescent molecular clouds in the disk of the Galaxy.

In Figure 3 we explore the same effects but now scale *both* the CR flux and the FUV ambient radiation field, since their *average* values are expected to rise in tandem in realistic star forming environments. In this case enhanced CII production at large FUV intensities

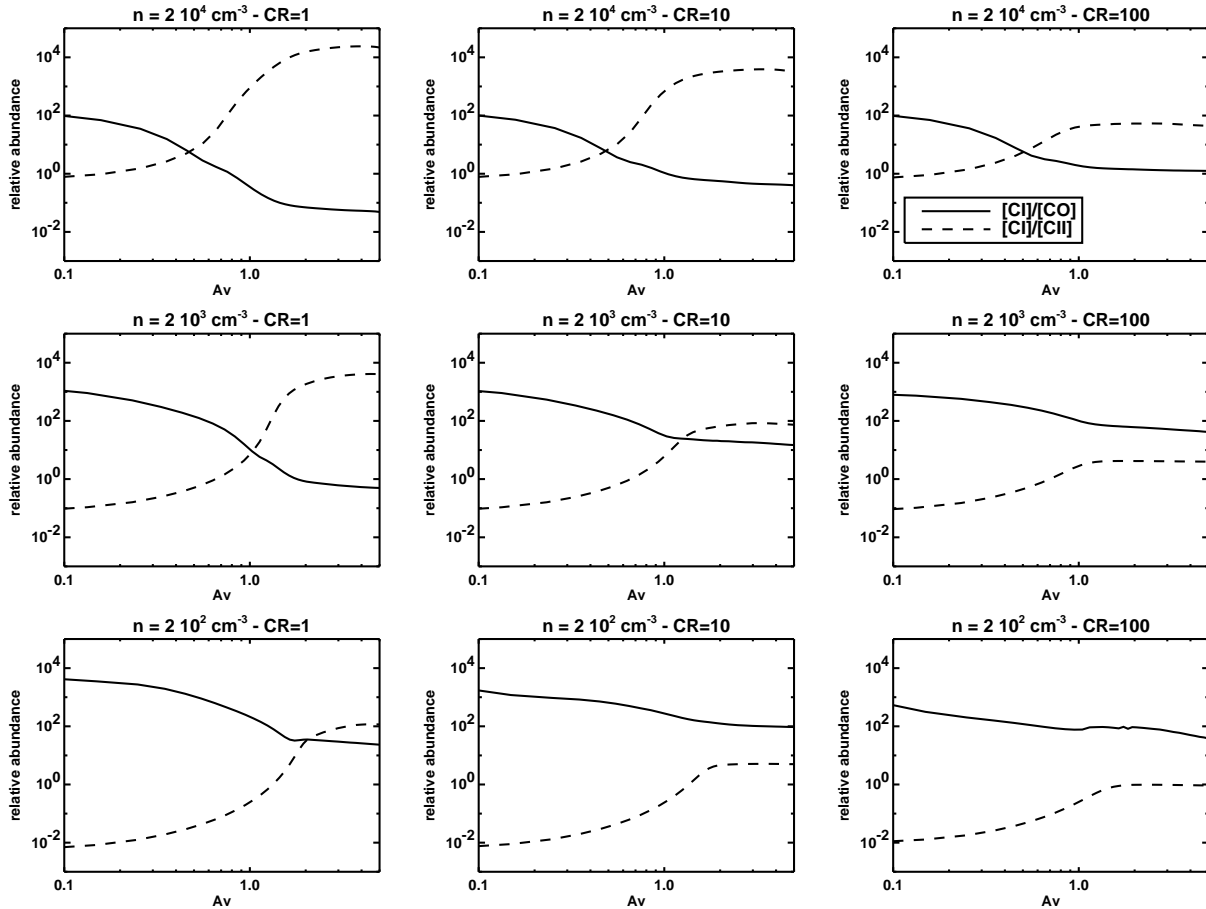


**Figure 2.** Abundance distributions at  $t = 10^7$  yrs, for identical initial conditions as in Figure 1. The values of  $F_{\text{CR}}$  are indicated in the panels, normalized to the Galactic value. The ambient  $G_0 = 1/2$ , corresponding to one-sided cloud illumination by a Habing field. In most cases  $[\text{CI}]/[\text{CII}] \gtrsim 1$  for  $A_v \gtrsim 1$ . The density range chosen characterizes the bulk of  $\text{H}_2$  in typical GMCs.

limits the cloud volume where CI is dominant, but except for diffuse gas irradiated by strong fields, CI remains the dominant form of carbon for  $A_v \gtrsim 2$ .

## 2.4 CI distribution in metal-poor environments

The expected evolution of metallicity in galaxies with an overall trend of lower values at earlier epochs is now verified by numerous observations (e.g. Mehlert et al. 2002). A trend of higher star formation rates in galaxies at higher redshifts is also deduced, although the details are far from clear (e.g. Ellis 2001; Somerville, Primack, & Faber 2001). It is therefore anticipated that galaxies with low metallicity and elevated star formation rates (and thus FUV and CR flux), will be common at high redshifts. Ly-break galaxies found at  $z \sim 3$  with moderate star formation rates of  $\sim (5 - 10) M_{\odot} \text{yr}^{-1}$  (Steidel et al. 1996), and sub-solar metallicities (e.g. Pettini et al. 2000) are typical such objects.

In low-metallicity environments with pervasive FUV radiation powered by star forma-

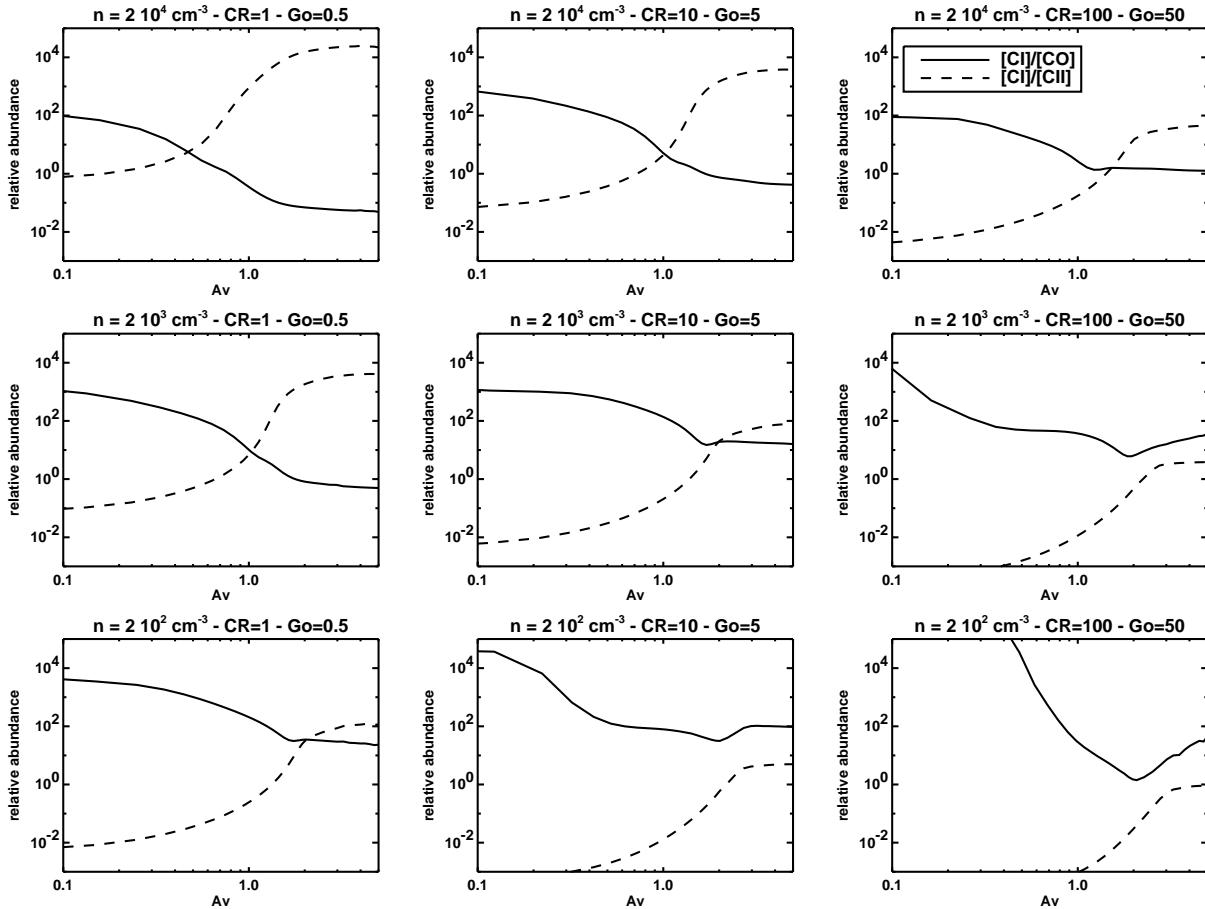


**Figure 3.** Abundance distributions at  $t = 10^7$  yrs, assuming the same initial conditions as in Figure 1. The values of  $F_{CR}$  are indicated in the panels, normalized to the Galactic value. The ambient  $G_0$  is now scaled proportionally but also multiplied by  $1/2$  corresponding to one-sided cloud illumination.

tion, the enhanced CO photodissociation diminishes its spatial extent per molecular cloud and thus its  $H_2$ -tracing capability (Pak et al. 1998; Bolatto, Jackson, & Ingalls 1999). Observational work using the AST/RO facility in the South Pole Station confirms these expectations by finding enhanced  $CI/^{12}CO$   $J=1-0$  line ratios in the LMC and SMC (Stark et al. 1997; Bolatto et al. 2000a). These data, albeit sparse and with a large dispersion, suggest  $I_{CI}/I_{CO} \propto Z^{-1/2}$ , supported also by observations in the low-metallicity star forming irregular IC 10 (Bolatto et al. 2000b and references therein).

In Figure 4 the effects of such conditions on the CI distribution in solar and sub-solar metallicity environments are contrasted, and it can be seen that CI remains the dominant form of carbon for the bulk of the cloud ( $A_v \geq 2$ ) even in the metal-poor case. *Thus in the metal-poor and modestly FUV-enhanced environments, characterizing many galaxies at high redshifts, CI remains a good tracer of molecular gas mass.*

A large change is seen however in the distribution of CII that now, unlike in the metal-

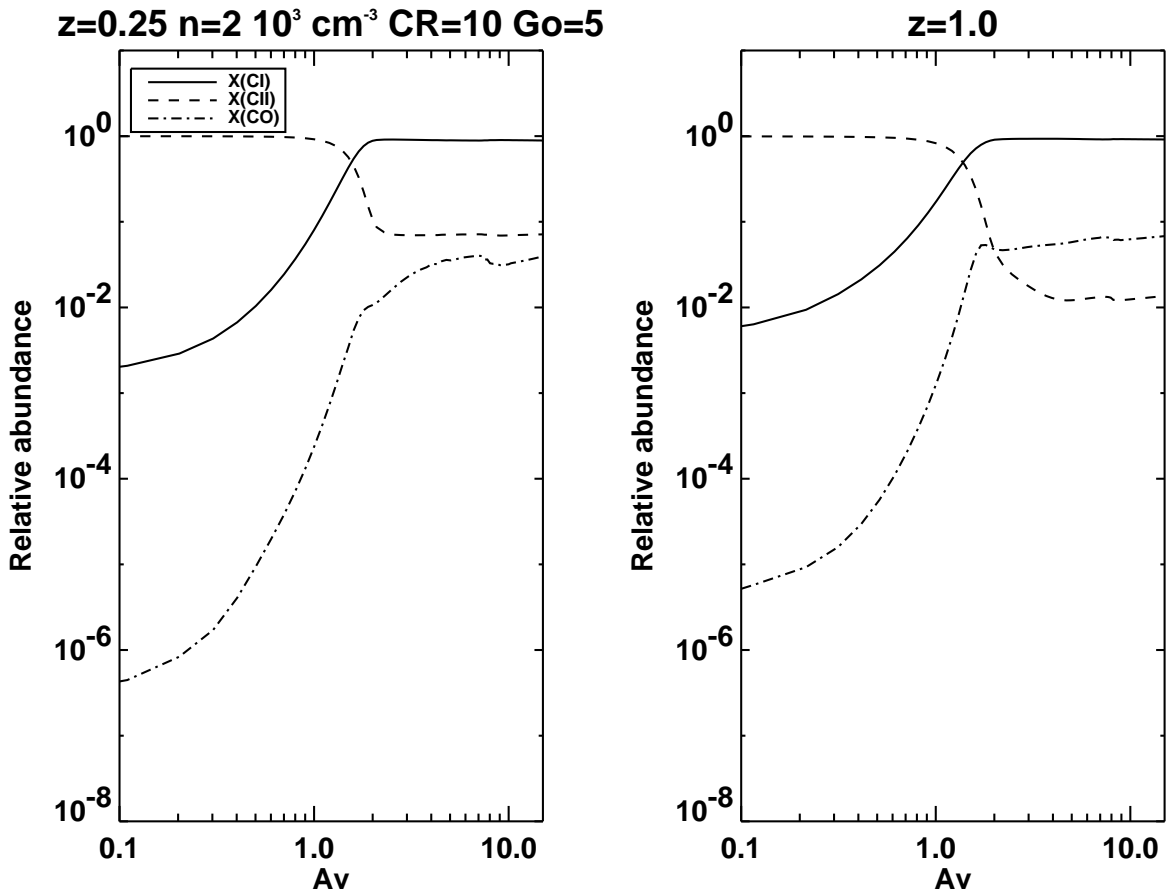


**Figure 4.** Carbon species abundance distributions at  $t = 10^7$  yrs relative to the total carbon content. The cloud is assumed initially atomic, and  $F_{\text{CR}}$ ,  $G_0$  correspond to an underlying star formation rate of  $\sim 10M_{\odot} \text{ yr}^{-1}$ , typical of Ly-break galaxies. The sub-solar metallicity of  $Z=0.25$  is also typical for Ly-break galaxies (Pettini et al. 2000).

rich case, it becomes more abundant than CO even deep into the cloud (yet still less than CI). Apart from the enhanced FUV photoionization of CI at low  $A_v$ 's, caused by the reduced dust shielding, low metallicity further enhances CII at the deeper parts of such clouds at the expense of CO because the main route of CO destruction at high  $A_v$  is via the reaction path:  $\text{CO} + \text{He}^+ \rightarrow \text{C}^+ + \text{O} + \text{He}$ . Once formed, ionized carbon will capture an electron from a metal atom in the gas phase but at low metallicities the charge exchange reactions involving the metallic atoms and ions are less efficient in converting  $\text{C}^+$  into C while  $\text{He}^+$  is formed in large abundance by the larger cosmic rays flux and thus a significant part of the carbon will be in the form of CII even at large  $A_v$ 's.

### 3 THE INTENSITY OF THE CI LINES

The critical densities of the fine structure CI lines  $^3P_1 \rightarrow ^3P_0$  ( $\nu_{10} = 492.160$  GHz) and  $^3P_2 \rightarrow ^3P_1$  ( $\nu_{21} = 809.343$  GHz) are  $n_{10} \sim 500 \text{ cm}^{-3}$  and  $n_{21} \sim 10^3 \text{ cm}^{-3}$ , comparable to those of the widely observed  $^{12}\text{CO}$  J=1–0, 2–1 transitions, while their upper energy levels are  $E_1/k = 23.6$  K, and  $E_2/k = 62.4$  K. The velocity-integrated flux density of a line is

$$\int_{\Delta v} S_x dV = \frac{2k\nu_x^2}{c^2} \left( \frac{1+z}{D_L^2} \right) L_x, \quad (4)$$

where  $D_L = 2cH_0^{-1}(1+z - \sqrt{1+z})$  is the luminosity distance for a redshift  $z$ ,  $L_x$  is the area/velocity-integrated line brightness temperature (in  $\text{K km sec}^{-1} \text{ pc}^2$ ), and  $\nu_x$  its rest-frame frequency. Hence, for any of the CI J=1–0, 2–1 and the  $^{12}\text{CO}$  J+1→J lines the velocity-integrated flux density ratio is

$$\frac{\int_{\Delta v} S_{\text{CI}} dV}{\int_{\Delta v} S_{\text{CO}} dV} = \left( \frac{\nu_{\text{ci}}}{\nu_{\text{co}}} \right)^2 \frac{R_{\text{CI}}}{R_{\text{J+1,J}}}, \quad (5)$$

where  $R_{\text{CI}} = \langle T_b(\text{CI}) \rangle / \langle T_b(\text{CO}_{1-0}) \rangle$ , and  $R_{\text{J+1,J}} = \langle T_b(\text{J}+1, \text{J}) \rangle / \langle T_b(1, 0) \rangle$  for  $^{12}\text{CO}$ . The brightness temperature averages are over velocity and emitting area.

An unresolved (or barely resolved) object, whose various ISM lines are accessible by a multiplicity of receivers, will have an observed CI flux density larger by the  $(\nu_{\text{ci}}/\nu_{\text{co}})^2$  factor relative to that of lower frequency CO transitions. Interferometric scaled-array observations ‘synthesizing’ the same beamsizes at widely different frequencies while utilizing the same collecting area maintain this advantage in the case of resolved objects. A flux density advantage of a CI line may remain even when  $\nu_{\text{ci}}/\nu_{\text{co}} \lesssim 1$ , simply because CI lines are much easier to excite and thus can maintain their intensities intact for diffuse and cooler gas while the  $R_{\text{J+1,J}}$  ratios diminish (see also Kaufman 1999). For example the  $^{12}\text{CO}$  J=4–3 and J=7–6 lines have critical densities  $n_{43} = 2 \times 10^4 \text{ cm}^{-3}$ ,  $n_{76} = 3 \times 10^6 \text{ cm}^{-3}$  and  $E_4/k \sim 55$  K,  $E_7/k \sim 155$  K, all much higher than the corresponding quantities of the CI J=1–0, 2–1 lines emitted at similar frequencies.

Thus for any *detected*  $^{12}\text{CO}$  J+1→J ( $J+1 \geq 3$ ) line, *bright CI emission may also be present, particularly for sub-thermally excited, and/or cooler gas (low  $R_{\text{J+1,J}}$ )*. This is of particular importance for the mounting number of high redshift ( $z \gtrsim 2$ ) CO detections, where only the  $J+1 \geq 3$  lines are usually observed while for such redshifts the CI lines no longer undergo large atmospheric absorption.

In Table 1 we summarize the typical brightness temperature line ratios measured in various ISM environments in the local Universe gleaned from an extensive search in the

literature. Large atmospheric absorption has prevented any large surveys of  $^{12}\text{CO}$   $J+1\rightarrow J$ ,  $J+1>3$  or  $^{13}\text{CO}$   $J=3-2$ , so we use a single-phase Large Velocity Gradient (LVG) code, constrained by the CO line ratios available in each case, to estimate expected flux densities for  $J+1>3$ . The results are then used to calculate detection advantage ratios  $D_a$ , defined as the signal-to-noise (S/N) ratio normalized by that of  $^{12}\text{CO}$   $J=1-0$  for equal integration time and velocity resolution. A general expression for the system sensitivity is

$$\delta S_{\text{rms}} = (\tau \Delta \nu)^{-1/2} \Delta S_{\text{sys}} = \left[ \frac{c}{\nu \tau_{\text{int}} \Delta V} \right]^{1/2} \Delta S_{\text{sys}}(\nu), \quad (6)$$

where  $\nu = (1+z)^{-1}\nu_x$  is the observed frequency of the line,  $\tau_{\text{int}}$  is the integration time,  $\Delta V$  is the velocity resolution, and  $\Delta S_{\text{sys}}(\nu)$  describes the overall system sensitivity and incorporates instrumental (e.g. collecting area, receiver temperatures) as well as atmosphere-dependent factors (e.g. absorption, signal decorrelation factors in case of interferometers).

From Equations 4 and 6 the S/N can be expressed as

$$\frac{\langle S_\nu \rangle_{\Delta V}}{\delta S_{\text{rms}}} = 2k \left( \frac{\nu}{c} \right)^{5/2} \langle T_b \rangle \left[ \frac{(1+z)^3}{D_L^2} \right] \frac{(\tau_{\text{int}} \Delta V)^{1/2}}{\Delta S_{\text{sys}}(\nu)}, \quad (7)$$

where  $\langle T_b \rangle$  is the velocity/area-averaged line brightness temperature. For frequencies of  $\sim 30-250$  GHz and future modern instruments like ALMA, located in dry sites,  $\Delta S_{\text{sys}}(\nu)/\nu^{1/2}$  changes  $\lesssim 50\%$ <sup>1</sup>. Thus setting  $\Delta S_{\text{sys}}(\nu) \propto \nu^{1/2}$ , and for a common  $\tau_{\text{int}}$  and  $\Delta V$ ,

$$D_a = \frac{(S/N)}{(S/N)_{\text{CO}(1-0)}} = (\nu_x/\nu_{10})^2 R \quad (8)$$

expresses the detection advantage of any spectral line with rest-frame frequency  $\nu_x$ , normalized to  $^{12}\text{CO}$   $J=1-0$ , with  $R$  being their brightness temperature ratio. This assumes a bandwidth fully covering both lines under comparison, which will be true for planned mm/sub-mm telescopes.

The  $D_a$  values for the  $^{12}\text{CO}$  and CI lines are shown in Figure 5 where it is obvious that  $^{12}\text{CO}$   $J=4-3$  marks a broad excitation ‘‘turnover’’ beyond which  $D_a(^{12}\text{CO})$  starts declining. This is not surprising since for most of the gas in GMCs  $T_{\text{kin}} \lesssim 50$  K, and  $n(\text{H}_2) \lesssim 10^4 \text{ cm}^{-3}$ , rendering the  $^{12}\text{CO}$   $J+1\rightarrow J$ ,  $J \geq 3$  lines sub-thermally excited and underluminous. The wide range of  $D_a(\text{CI})$  values reflects the considerable range of  $R_{\text{CI}}$  ratios observed in various environments, which is not simply correlated to that of the  $^{12}\text{CO}$  line ratios, e.g. a large  $R_{J+1,J}$  not necessarily mean also a large  $R_{\text{CI}}$ . The CI  $J=1-0$  line has a clear advantage over  $^{12}\text{CO}$  transitions in quiescent environments and maintains a sizable one in starbursts. The

<sup>1</sup> See <http://www.alma.nrao.edu/info/sensitivities>, Table 1

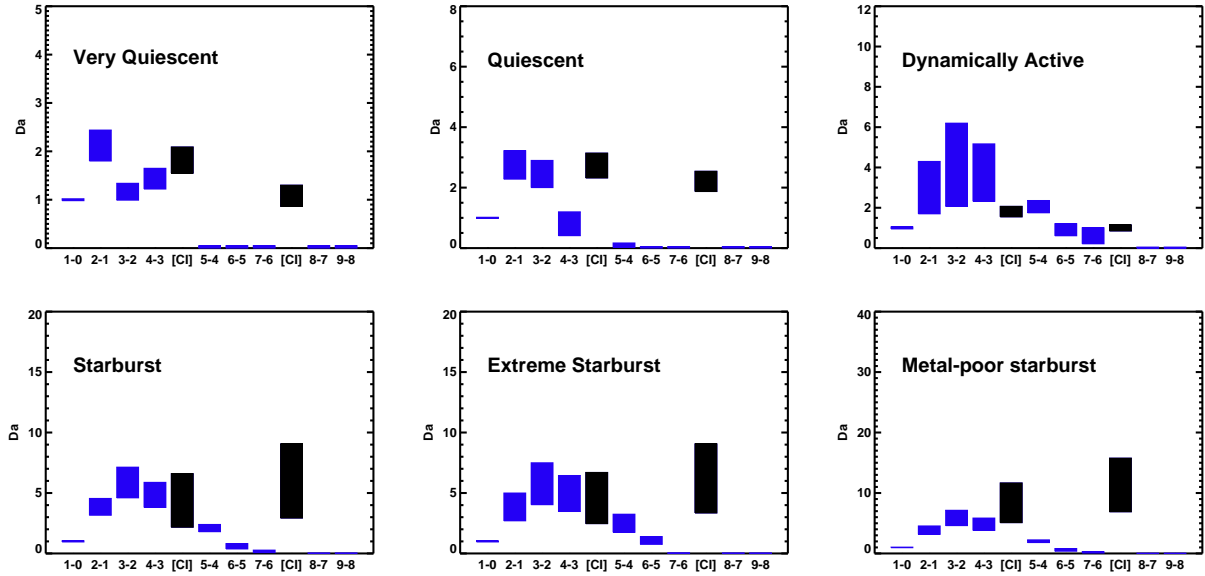


**Figure 5.** The values of  $D_a$  for the ISM environments listed in Table 1 (see text). A dispersion of  $\sim 15\%$  was assumed for all ratios (typical error of the mean value reported by surveys). For dynamically active and extreme starburst environments we adopt the much larger range of the CO line ratios found around the mean values reported in Table 1. For metal-poor starburst we set  $Z=0.25$ , and adopt the scaling  $R_{\text{CI}}(Z) = Z^{-1/2}R_{\text{CI}}(1)$  (Bolatto et al. 2000b), all other ratios are assumed the same as in starbursts.

CI  $J = 2 - 1$  is the only line in the molecular ISM that maintains high  $D_a$  at such high frequencies under most conditions, a conclusion subject to the uncertainty of the assumed  $\text{CI}(2 - 1)/(1 - 0)$  ratio which has not been widely measured. For metal-poor starbursts Figure 5 can be somewhat misleading since in such environments CII may dominate over the bulk of the molecular gas mass with both the  $^{12}\text{CO}$  and CI lines being rather weak. Nevertheless in the case of a *detected*  $^{12}\text{CO}$  line in such an environment, CI line emission is expected to be bright as well.

It must be emphasized that  $D_a$  values translate to a practical observational advantage provided the relevant lines do not fall near any of the (many) atmospheric absorption windows within the 30–250 GHz frequency range, and that the set of  $^{12}\text{CO}$ , CI lines under comparison is accessible within this frequency interval. The latter implies redshifts of  $z_{1-0} \gtrsim 1$  and  $z_{2-1} \gtrsim 2.25$  so that the CI  $J=1-0$ ,  $2-1$  lines fall within the aforementioned range.

A *single* receiver observing various molecular ISM lines redshifted within its tuning range from several objects distributed over a redshift range is a case more relevant to current instrumentation capabilities (limited set of receivers per telescope) and blank field spectral line surveys to be conducted with future instruments per observing band (e.g. Blain et al. 2000). Then Equation 8 is no longer relevant and one has to simply look at Equation 7 and the expression in the brackets which changes  $\lesssim 3\%$  for  $z \sim 1 - 10$ . This allows  $^{12}\text{CO}$ , CI lines to trace similar amounts of gas mass over a progressively larger redshift range as long as sufficiently excited lines with progressively larger rest-frame frequencies become accessible. This is simply the spectral-line equivalent of the well-known favorable K-correction that keeps the FIR/sub-mm dust continuum of galaxies undiminished (and thus detectable) over a large range of redshifts. For  $^{12}\text{CO}$  lines this is beautifully demonstrated by  $^{12}\text{CO}$  J=1 – 0 observations of nearby QSOs that measure  $\text{H}_2$  masses similar to those found in high redshift QSOs and radio galaxies detected through higher-J  $^{12}\text{CO}$  lines (Evans et al. 2001).

Studies examining the luminosity of molecular and atomic ISM lines in the context of emission-line searches at high redshifts (e.g. Blain et al. 2000) do not explore the  $\text{H}_2$ -tracing potential of the CI lines. Moreover, by making favorable assumptions about the gas excitation they present optimistic predictions of flux densities, particularly for high-J  $^{12}\text{CO}$  transitions. This is why some of their brightness temperature line ratios are unrealistic, e.g.  $\text{CI}(2-1)/(1-0) \sim 2.25$  (Table 1 in Blain et al. 2000), while the highest value observed to date is  $\sim 1$ , in M 82 (Stutzki et al. 1997) and the Orion KL region (Yamamoto 2001).

There is no reason to believe that the variety of environments indicated in Figure 5 will not be also present at high redshifts. Even if starburst environments are more frequently encountered there, the possibility of large scale sub-thermal excitation as suggested by recent measurements in the extremely red object (ERO) and starburst HR 10 at  $z \sim 1.45$  (Greve et al. 2003), cannot be discounted. The excitation turnover at the frequencies of the CI J=1–0 and  $^{12}\text{CO}$  J=4–3 lines implies that, with the exception of the CI J=2–1 line, the gas mass tracing capability of higher frequency lines ( $\nu > 492$  GHz) is suppressed except in star-forming environments. For essentially the same reasons molecular gas mass estimates based solely on high-J  $^{12}\text{CO}$  lines observed at high redshifts carry large uncertainties (factors of  $\gtrsim 10$ ). Summarizing, while metal-rich gas fueling star-formation is bound to figure prominently in high-J  $^{12}\text{CO}$  line emission at high redshifts, it will not be the only gas phase present and large amounts of colder, diffuse molecular gas may be lingering e.g. “in-between” successive star forming events beyond the current star-forming sites.



Here we must mention that the case for observing the low <sup>12</sup>CO J=1–0, 2–1 lines remains strong even if the CI lines can deliver more flux per H<sub>2</sub> mass for e.g. cool and diffuse gas reservoirs. This is because of the current commissioning of large single dish radio telescopes like the Green Bank Telescope (GBT) (tunable up to 115 GHz), and future instruments as the expanded VLA (EVLA), (continuously tunable below 45 GHz), and a Square Kilometer Array (SKA) equipped with high frequency receivers (~ 20 – 45 GHz). These will be able to conduct very sensitive observations of the low-J <sup>12</sup>CO transitions at high redshifts (Carilli & Blain 2002), bypass the excitation biases mentioned previously, and sensitively trace molecular gas in the distant Universe.

#### 4 DEDUCING H<sub>2</sub> MASS FROM CI LINE INTENSITIES: THE UNCERTAINTIES

The CI lines have small to moderate optical depths ( $\tau_{\text{CI}} \sim 0.1 - 1$ ) being, over large scales, as optically thin as <sup>13</sup>CO (Ojha et al. 2001; Ikeda et al. 2002). This property along with their simpler 3-level partition function and easy thermalization makes them more straightforward H<sub>2</sub> gas mass tracers than the usually optically thick <sup>12</sup>CO lines.

For an optically thin line the emergent brightness is

$$I_{\nu_{\text{em}}} = \frac{h\nu_{\text{ul}}}{4\pi} A_{\text{ul}} N_{\text{u}} \phi_{\nu_{\text{em}}} \quad (9)$$

where  $N_{\text{u}}$  is the column density of the upper level, and  $\phi_{\nu_{\text{em}}}$  is the intrinsic line profile. The received brightness is  $I_{\nu} = (1+z)^{-3} I_{\nu_{\text{em}}}$  (see e.g. Ivison et al. 1996). Thus in terms of the usually reported observable  $I = \int S_{\nu} dV$  ( $S_{\nu} = \int I_{\nu} d\Omega$ ) the CI beam-averaged column density over the telescope beam  $\Omega_{\text{b}}$  can be expressed as

$$N_{\text{CI}} = \frac{4\pi(1+z)^3 I_{\text{CI}}}{hc A_{\text{ul}} Q_{\text{ul}} \Omega_{\text{b}}} \quad (10)$$

where the  $Q_{\text{ul}} = N_{\text{u}}/N_{\text{CI}} < 1$  excitation factor depends on ( $n$ ,  $T_{\text{k}}$ ), and the radiation field (see Appendix). In terms of the gas mass contained within  $\Omega_{\text{b}}$  the last expression becomes

$$M_{\text{A}_b} = \frac{4\pi\mu m_{\text{H}_2}}{hc A_{\text{ul}} X_{\text{CI}}} \left( \frac{D_{\text{L}}^2}{1+z} \right) Q_{\text{ul}}^{-1} I_{\text{CI}}, \quad (11)$$

where we used  $A_{\text{b}} = (1+z)^{-4} D_{\text{L}}^2 \Omega_{\text{b}}$  as the corresponding area of the beam at the redshift of the source,  $X_{\text{CI}} = [\text{C}]/[\text{H}_2]$ , and  $\mu = 1.36$  corrects for the mass in He. In astrophysical units,

$$\frac{M_{\text{A}_b}}{M_{\odot}} = 4.92 \times 10^{10} h'^{-2} \frac{(1+z - \sqrt{1+z})^2}{1+z} \left[ \frac{X_{\text{CI}}}{10^{-5}} \right]^{-1} \left[ \frac{A_{\text{ul}}}{10^{-7} \text{s}^{-1}} \right]^{-1} Q_{\text{ul}}^{-1} \left[ \frac{I_{\text{CI}}}{\text{Jy km s}^{-1}} \right], \quad (12)$$

where we set  $H_0 = 100h' \text{ km s}^{-1}\text{Mpc}^{-1}$

For optically thick emission the latter expression yields a lower limit on the gas mass and remains valid for optical depths emerging in radiatively decoupled “cells” much smaller than the emitting region, but with  $A_{ul}$  replaced by  $\beta_{ul}A_{ul}$  ( $\beta = (1 - e^{-\tau})/\tau$ : photon escape probability). In molecular clouds where  $\tau_{CI} \lesssim 1$ , an unknown value of  $\beta_{ul}$  introduces an uncertainty of  $\lesssim 60\%$ . A greater source of uncertainty stems from the assumed excitation conditions that determine  $Q_{ul}$ . For high redshift objects where only one or two lines are usually detected there can be no practical constraints on the gas excitation and the minimal assumption of LTE is usually made in order to deduce  $M(\text{H}_2)$ . For typical  $n = (100 - 5 \times 10^4) \text{ cm}^{-3}$  and  $T_k = (20 - 60) \text{ K}$  it is  $Q_{10}/Q_{10}^{(LTE)} \sim 0.35 - 1$  and  $Q_{21}/Q_{21}^{(LTE)} \sim 0.15 - 1$ . These uncertainties can be larger if there are no available temperature constraints from e.g. measurements of the dust continuum. Predictably  $Q_{21}$  has the largest variation, making the CI J=2–1 transition the more uncertain  $\text{H}_2$  mass estimator of the two CI lines. Nevertheless the  $^{12}\text{CO}$  J=7–6 line at a similar frequency (806 GHz) is much more sensitive to ambient conditions, and hence an even more uncertain  $\text{H}_2$  mass tracer. Similarly the CI J=1–0 with a smaller  $Q_{10}$  variation is tracing  $\text{H}_2$  gas more reliably than the  $^{12}\text{CO}$  J=4–3 (461 GHz) line even though the latter can be significantly stronger.

In deducing  $M(\text{H}_2)$  from CI lines we assumed CI distributed throughout a typical molecular cloud but also no significant “contamination” from any other gas phase. This is indeed the case since carbon in HI gas is mostly ionized with e.g.  $[\text{CI}]/[\text{CII}] \lesssim 3 \times 10^{-3}$  in the CNM phase (Wolfire et al. 2003). The small CI line optical depths are an advantage when estimating  $\text{H}_2$  mass but they also add  $X_{CI}$  to the list of uncertainties. Given the variety of processes affecting  $[\text{CI}]/[^{12}\text{CO}]$  and thus  $X_{CI}$ , it seems that the latter can vary widely. However *the very same processes also affect*  $X_{CO} = [^{12}\text{CO}]/[\text{H}_2]$ , which is nevertheless found to be relatively constant ( $\sim 10^{-4}$ ) over large scales for clouds with  $A_v \gtrsim 2$  (e.g. van Dishoeck 1992). This is in accordance with the constant  $N(\text{CI})/N(^{12}\text{CO}) \sim 0.1 - 0.2$  found by large scale CI,  $^{12}\text{CO}$ ,  $^{13}\text{CO}$  J=1–0 surveys (e.g. Ikeda et al 2002) and suggests a dominant physical process that along with turbulent diffusion sets a relatively constant  $[\text{C}]/[^{12}\text{CO}]$  throughout a GMC. However, as was the case for  $^{12}\text{CO}$ , establishing average  $X_{CI}$  values will probably be done observationally, with large surveys conducted over a broad range of conditions and discerning any general trends of  $[\text{C}]/[^{12}\text{CO}]$  (and thus  $X_{CI}$ ) in active and/or metal-poor environments.

## 5 OBSERVATIONAL PROSPECTS AT HIGH REDSHIFTS

The potential advantage of the CI lines as  $H_2$  mass tracers can be fully realized only at high redshifts. For  $z_{10} \gtrsim 1$  the CI J=1–0 line is redshifted to  $\lesssim 250$  GHz where a combination of existing large-aperture instruments (single dish and interferometers) and a much improved atmospheric transmission enables sensitive observations. For the J=2–1 transition the aforementioned limit is  $z_{21} \gtrsim 2.25$ , a typical redshift of the new population of sub-mm bright, starburst galaxies (Chapman et al. 2003). The commissioning of interferometers in excellent sites, namely SMA on Mauna Kea, Hawaii and ALMA in Llano de Chajnantor, Chile, will allow routine sensitive observations at sub-mm wavelengths. In such sites the atmospheric transmission even at  $\sim 345$  GHz remains exceptional most of the time ( $\sim 80\%$  at zenith, except around the 325 GHz atmospheric absorption feature), and the CI lines become accessible to sensitive measurements for  $z_{10} \gtrsim 0.4$  and  $z_{21} \gtrsim 1.3$ . Particularly interesting is the case when *both* CI lines become accessible at lower frequencies, thus allowing an estimate of gas temperatures from their intensity ratio (assuming LTE) independently of those based on dust continuum or  $^{12}\text{CO}$  transitions.

Currently all high redshift objects detected in  $^{12}\text{CO}$  are the sites of large scale starbursts and are good targets for CI observations, which hold the promise of uncovering  $H_2$  gas untraced by the high-J  $^{12}\text{CO}$  transitions. Recently an opportunity to drastically increase their rather small numbers has emerged with the successful spectroscopic redshift determination of several sub-mm bright starbursts at high redshifts (Chapman et al. 2003). Such objects are metal-rich and are found to be prominent  $^{12}\text{CO}$  emitters (e.g. Neri et al. 2003). The recent detection of weak  $^{12}\text{CO}$  J=3–2 in a Ly-break galaxy at  $z=2.7$  (Baker et al. 2003), with its CI J=2–1 line redshifted to  $\sim 218$  GHz, offers the possibility of testing the potential of CI lines as  $H_2$  gas tracers in metal-poor and modestly UV-intense objects.

The recent detection of massive gaseous disks at high redshifts (Genzel et al. 2003) are currently a highly contentious issue since their presence at such early epochs is hard to reconcile with standard hierarchical models of galaxy evolution. The much larger spatial distribution of the CI line emission with respect to high-J  $^{12}\text{CO}$  transitions in typical disks like the Milky Way, *holds the promise of yielding a much better picture of disk kinematics and total dynamical mass* (by encompassing its flat rotation curve part), and thus is an excellent alternative.

There are currently only two reported detections of CI lines at high redshifts, namely in

the Cloverleaf quasar ( $z=2.56$ ) (Barvainis et al. 1997; Weiss et al. 2003), and the IRAS galaxy F10214+472 ( $z=2.28$ ) (Brown & Vanden Bout 1992)<sup>2</sup>. Both are strongly lensed systems and particularities of differential lensing may be responsible for their very different CI/<sup>12</sup>CO flux density ratios. Clearly CI observations of non-lensed high redshift objects are needed.

Interestingly in the case of the Cloverleaf, and based on the assumption of a concomitant CI emission, Weiss et al. find an H<sub>2</sub> gas mass similar to that deduced from the well-sampled dust continuum or from the multi-transition <sup>12</sup>CO observations, lending support to the main argument of this work.

Finally, the markedly more difficult CI observations in the local Universe remain valuable since large scale CI, <sup>12</sup>CO, and <sup>13</sup>CO surveys in a variety of environments are needed to establish the range of X<sub>CI</sub> and “cross-calibrate” the two methods of estimating H<sub>2</sub> gas mass. It is particularly interesting to observe intensely star-forming and/or metal-poor objects in order to search for [C]/[<sup>12</sup>CO] enhancements and its possible metallicity dependence.

## 6 CONCLUSIONS

In this work we examined the prospects of using the two lines of atomic carbon at 492 GHz (J=1–0) and 809 GHz (J=2–1) as alternative H<sub>2</sub> mass tracers in galaxies. Our conclusions can be summarized as follows:

1. Non-equilibrium chemical states, turbulent diffusive mixing, and cosmic rays can easily make CI ubiquitous throughout a typical Giant Molecular Cloud. This is now firmly supported by large scale CI, <sup>12</sup>CO, <sup>13</sup>CO surveys of such clouds in the Milky Way, which also find a constant average [C]/[<sup>12</sup>CO] abundance ratio over the bulk of their mass.

2. In star forming and/or dynamically fast-evolving environments the processes responsible for the ubiquity of CI in GMCs will further enhance its abundance. In UV-intense and metal-poor objects large scale CII production diminishes the H<sub>2</sub>-tracing capability of CI, which nevertheless remains better than that of the now severely dissociated <sup>12</sup>CO.

3. In terms of emerging flux density as a function of excitation conditions CI lines have a potentially strong advantage with respect to <sup>12</sup>CO lines in tracing H<sub>2</sub> gas mass under diffuse and/or cooler conditions as well as in the metal poor environments of mild starbursts. However the large atmospheric absorption at their rest-frame frequencies allows such an advantage to materialize at high redshifts ( $z \gtrsim 1$ ).

<sup>2</sup> This detection was under dispute but it has been recently confirmed (Papadopoulos et al. 2004)

4. The simpler 3-level structure of the CI lines, their small optical depths and modest excitation requirements with respect to  $^{12}\text{CO}$  lines of similar frequency make the associated  $H_2$  mass estimates more straightforward. However the usually unknown (particularly for high redshift sources) mean excitation conditions introduce large uncertainties in such estimates, which are reduced considerably if an estimate of the gas temperature is available.

5. Concentrated observational effort in the local Universe remains critical. Large scale CI,  $^{12}\text{CO}$ , and  $^{13}\text{CO}$  surveys of GMCs in a variety of environments will help address issues of optical depths,  $[\text{CI}]/[\text{H}_2]$  abundances and its variations, and “cross-calibrate” the two  $H_2$  gas mass tracing techniques.

## ACKNOWLEDGMENTS

We thank A. Weiss for a detailed reading of the original manuscript and critical comments that have greatly improved it. Comments by the anonymous referee are gratefully acknowledged. P.P.P. thanks Arjen van der Wel for fruitful discussions and acknowledges the support of a Marie Curie Individual Fellowship HPMT-CT-2000-00875.

**Table 1.** CO, CI line ratios, typical LVG solutions

Environment <sup>a</sup>	R <sub>21</sub> <sup>b</sup>	R <sub>32</sub> <sup>b</sup>	K <sub>10</sub> <sup>c</sup>	K <sub>21</sub> <sup>c</sup>	R <sub>ci</sub> (r <sub>21</sub> ) <sup>d</sup>	LVG solutions <sup>e</sup>	References
Very quiescent	0.4	0.15	9	....	0.10 (0.22)	10, 10 <sup>3</sup> , 10 <sup>-5</sup> (40) 10, 300, 10 <sup>-4</sup> (60)	1, 2, 3, 4
Quiescent	0.6	0.30	5	....	0.15 (0.30)	20, 300, 10 <sup>-4</sup> (40) 10, 10 <sup>3</sup> , 3 × 10 <sup>-5</sup> (60)	5, 6, 7, 8
Dynamically active	0.95	....	10	10	0.10 (0.22)	60, 10 <sup>3</sup> , 10 <sup>-5</sup> (25)	9, 10, 11, 12
Starburst	0.95	0.65	15	15	0.15-0.30 (0.5)	30, 300, 3 × 10 <sup>-6</sup> (40) <sup>f</sup> 60, 10 <sup>3</sup> , 10 <sup>-5</sup> (40)	13, 14, 15, 16, 17
Extreme starburst <sup>g</sup>	0.95	0.65	25	25	0.15-0.30 (0.5)	70, 10 <sup>3</sup> , 10 <sup>-5</sup> (60)	13, 14

<sup>a</sup> Very quiescent: M31 cold clouds, Quiescent: Milky Way disk, Dynamically active: Galactic Center, Starburst: various line surveys in several objects, Extreme starbursts: ULIRG nuclei

<sup>b</sup> The <sup>12</sup>CO (2-1)/(1-0), (3-2)/(1-0) brightness temperature ratios

<sup>c</sup> The <sup>12</sup>CO/<sup>13</sup>CO brightness temperature ratios for J=1-0, 2-1

<sup>d</sup> The <sup>12</sup>CO/CI J=1-0 and r<sub>21</sub>=CI(2-1)/(1-0) brightness temperature ratios

<sup>e</sup> LVG solutions: T<sub>k</sub>(K), n(H<sub>2</sub>)(cm<sup>-3</sup>), X<sub>CO</sub>/(dV/dr)([km s<sup>-1</sup>pc<sup>-1</sup>]<sup>-1</sup>), ([<sup>12</sup>CO/<sup>13</sup>CO] = 40, 60), X<sub>CO</sub> = [<sup>12</sup>CO/H<sub>2</sub>]. In case of serious “degeneracies” typical solutions from both parts of the parameter space are displayed (e.g. in starbursts).

<sup>f</sup> Best solutions occur for [<sup>12</sup>CO/<sup>13</sup>CO] = 40

<sup>g</sup> Indicative ratios only, large range of values observed we adopt the R<sub>32</sub> and CI values from starbursts.

1: Israel, Tilanus, & Baas 1998, 2: Allen et al. 1999 (*COBE*, outer Galaxy), 4: Wilson 1997 (M 33 clouds), 5: Disk cloud surveys by Chiar et al. 1994; Hasegawa 1997; Sakamoto et al. 1997; Falgarone et al. 1998; Sanders et al. 1993 (for CO 3-2); Digel, de Geus, & Thaddeus 1994, 6: Disk cloud surveys by Solomon, Scoville, & Sanders 1979; Rickard & Blitz 1985; Polk et al. 1988; Falgarone et al. 1998; Wilson et al. 1999, 7: Fixsen et al. 1999 (inner Galaxy); 8: Gerin & Philips 2000; 9: Langer & Penzias 1993; 10: Sawada et al. 2001; 11: Ojha et al. 2001; 12: Fixsen et al. 1999 (Galactic center); 13: Braine & Combes 1992, Aalto et al. 1995, Papadopoulos & Seaquist 1998; 14: Devereux et al. 1994; 15: Stutzki et al. 1997; Yamamoto et al. 2001; 16: Israel, White, & Baas 1995, Petitpas & Wilson 1998; Israel & Baas 2002, 17: Stark et al. 1997; Bolatto et al. 2000a, 2000b

**APPENDIX A: THE 3-LEVEL SYSTEM AND THE CI LINES**

The rate equations for a 3-level system in steady state under the assumption of  $A_{20}/A_{21} \ll 1$ ,  $A_{20}/A_{10} \ll 1$ , as is the case for the CI fine structure levels, are

$$\frac{dn_2}{dt} = B_{12}J_{\nu_{21}}n_1 - (B_{21}J_{\nu_{21}} + A_{21})n_2 + [C_{12}n_1 + C_{02}n_0 - C_{21}n_2 - C_{20}n_2] = 0, \quad (A1)$$

$$\begin{aligned} \frac{dn_1}{dt} = (B_{21}J_{\nu_{21}} + A_{21})n_2 + B_{01}J_{\nu_{10}}n_0 - (A_{10} + B_{10}J_{\nu_{10}} + B_{12}J_{21})n_1 + \\ [C_{21}n_2 + C_{01}n_0 - C_{12}n_1 - C_{10}n_1] = 0, \end{aligned} \quad (A2)$$

where  $J_\nu = 2h\nu^3/c^2 [\exp(h\nu/kT_b) - 1]^{-1}$  is the background radiation field (assumed isotropic and with no line contribution),  $C_{ul} = n\gamma_{ul}$  are the rates of collisional de-excitation ( $u \rightarrow l$ ) related to those of the reverse process through the principle of detailed balanced  $C_{lu}/C_{ul} = (g_u/g_l)\exp(-h\nu_{ul}/kT_k)$ . The term in the square brackets is the net collisional population/depopulation of the levels, and the rest are the stimulated and spontaneous processes.

The stimulated excitation and de-excitation coefficients are related as  $g_u B_{ul} = g_l B_{lu}$  and to the spontaneous emission coefficient  $A_{ul} = (2h\nu_{ul}^3/c^2)B_{ul}$ . The latter can be used to demonstrate that  $B_{20}/B_{21} \ll 1$  and  $B_{20}/B_{10} \ll 1$ , also assumed in the previous equations. After some reordering and replacing all the  $B_{ik}$  factors we get

$$(C_{21} + C_{20} + f_{21}A_{21})n_2 - [C_{12} + g_2/g_1(f_{21} - 1)A_{21}]n_1 - C_{02}n_0 = 0, \quad (A3)$$

$$\begin{aligned} (C_{21} + f_{21}A_{21})n_2 - [C_{10} + C_{12} + f_{10}A_{10} + g_2/g_1(f_{21} - 1)A_{21}]n_1 + \\ [C_{01} + g_1/g_0(f_{10} - 1)A_{10}]n_0 = 0, \end{aligned} \quad (A4)$$

with  $f = \exp(h\nu/kT_b)/[\exp(h\nu/kT_b) - 1]$ . Equations A3, A4 along with the ‘‘closure’’ relation

$$n_2 + n_1 + n_0 = n_{CI}, \quad (A5)$$

are used to solve for the level populations. We find the following expressions,

$$\begin{aligned} \frac{n_1/n_{CI}}{K^{-1}} = 1 + f_{21} \left(1 + \frac{C_{20}}{C_{21}}\right) \frac{n_{21}}{n} + \frac{C_{01}}{C_{02}} \left(1 + \frac{C_{20}}{C_{21}}\right) \left(1 + f_{21} \frac{n_{21}}{n}\right) \times \\ \left[1 + \frac{g_1}{g_0}(f_{10} - 1) \left(\frac{C_{12} + C_{10}}{C_{01}}\right) \frac{n_{10}}{n}\right], \end{aligned} \quad (A6)$$

$$\frac{n_2/n_{\text{CI}}}{K^{-1}} = \left(1 + f_{10} \frac{n_{10}}{n}\right) \frac{C_{10} + C_{12}}{C_{21}} + \frac{g_2}{g_1} (f_{21} - 1) \left(1 + \frac{C_{20}}{C_{21}}\right) \frac{n_{21}}{n} + \frac{C_{10}}{C_{20}} \times \left[1 + \frac{g_2}{g_1} (f_{21} - 1) \left(\frac{C_{21} + C_{20}}{C_{12}}\right) \frac{n_{21}}{n}\right] \times \left[1 + \frac{g_1}{g_0} (f_{10} - 1) \left(\frac{C_{10} + C_{12}}{C_{01}}\right) \frac{n_{10}}{n}\right], \quad (\text{A7})$$

and

$$\frac{n_0/n_{\text{CI}}}{K^{-1}} = \frac{C_{10}}{C_{02}} \left(1 + f_{21} \frac{n_{21}}{n}\right) \left(1 + \frac{C_{20}}{C_{21}}\right) \left[1 + f_{10} \left(1 + \frac{C_{12}}{C_{10}}\right) \frac{n_{10}}{n}\right] + \frac{C_{10}}{C_{01}} \times \left[1 + \frac{g_2}{g_1} (f_{21} - 1) \left(\frac{C_{20} + C_{21}}{C_{12}}\right) \frac{n_{21}}{n}\right] \quad (\text{A8})$$

It is  $Q_{10} = n_1/n_{\text{CI}}$  and  $Q_{21} = n_2/n_{\text{CI}}$  (see main text) while the critical density of a transition  $u \rightarrow l$  is  $n_{\text{ul}} = A_{\text{ul}} / (\sum_k \gamma_{\text{uk}})$  (e.g. Jansen 1995), where the sum is over all collisional processes out of the level (u). In the literature often only the  $\gamma_{\text{ul}}$  coefficient or the sum of just the downwards rates is used resulting to an often serious overestimate of  $n_{\text{ul}}$ . For the 3-level atom it is  $n_{21} = A_{21} / (\gamma_{20} + \gamma_{21})$  and  $n_{10} = A_{10} / (\gamma_{12} + \gamma_{10})$  ( $n_{10} > n_{21}$ ). The expression for K is given by

$$K = 1 + \left(1 + \frac{C_{20}}{C_{21}}\right) \left\{ \left(f_{21} + \frac{g_2}{g_1} (f_{21} - 1)\right) \frac{n_{21}}{n} + \frac{C_{10}}{C_{02}} \left(1 + f_{21} \frac{n_{21}}{n}\right) \left(1 + \frac{C_{01}}{C_{10}}\right) \times \left[1 + \left(f_{10} + \frac{g_1}{g_0} (f_{10} - 1)\right) \left(\frac{C_{10} + C_{12}}{C_{01} + C_{10}}\right) \frac{n_{10}}{n}\right] \right\} + \left(1 + f_{10} \frac{n_{10}}{n}\right) \frac{C_{12} + C_{10}}{C_{21}} + \frac{C_{10}}{C_{01}} \left(1 + \frac{C_{01}}{C_{20}}\right) \times \left[1 + \frac{g_2}{g_1} (f_{21} - 1) \left(\frac{C_{20} + C_{21}}{C_{12}}\right) \frac{n_{21}}{n}\right] \times \left[1 + \frac{g_1}{g_0} (f_{10} - 1) \left(\frac{C_{10} + C_{12}}{C_{20} + C_{01}}\right) \frac{n_{10}}{n}\right]. \quad (\text{A9})$$

In the case  $n_{21}/n \rightarrow 0$  (and thus also  $n_{10}/n \rightarrow 0$ ), the last expressions yield

$$\frac{n_1/n_{\text{CI}}}{K^{-1}} \rightarrow 1 + \left(1 + \frac{C_{20}}{C_{21}}\right) \frac{C_{01}}{C_{02}} = 1 + \frac{C_{01}}{C_{02}} + \frac{C_{10}}{C_{12}}, \quad (\text{A10})$$

$$\frac{n_2/n_{\text{CI}}}{K^{-1}} \rightarrow \frac{C_{10} + C_{12}}{C_{21}} + \frac{C_{10}}{C_{20}} = \frac{C_{12}}{C_{21}} \left(1 + \frac{C_{01}}{C_{02}} + \frac{C_{10}}{C_{12}}\right), \quad (\text{A11})$$

and

$$\frac{n_0/n_{\text{CI}}}{K^{-1}} \rightarrow \left(1 + \frac{C_{20}}{C_{21}}\right) \frac{C_{10}}{C_{02}} + \frac{C_{10}}{C_{01}} = \frac{C_{10}}{C_{01}} \left(1 + \frac{C_{01}}{C_{02}} + \frac{C_{10}}{C_{12}}\right). \quad (\text{A12})$$

The last relations yield

$$\frac{n_2}{n_1} = \frac{C_{12}}{C_{21}} = \frac{g_2}{g_1} e^{-E_{21}/kT_k}, \quad \text{and} \quad \frac{n_1}{n_0} = \frac{C_{01}}{C_{10}} = \frac{g_1}{g_0} e^{-E_{10}/kT_k}, \quad (\text{A13})$$

which are the LTE values while the expression for K becomes



$$K \rightarrow 1 + \left(1 + \frac{C_{20}}{C_{21}}\right) \left(1 + \frac{C_{01}}{C_{10}}\right) \frac{C_{10}}{C_{02}} + \frac{C_{12} + C_{10}}{C_{21}} + \frac{C_{10}}{C_{01}} \left(1 + \frac{C_{01}}{C_{20}}\right) = \left(1 + \frac{C_{01}}{C_{02}} + \frac{C_{10}}{C_{12}}\right) \left(1 + \frac{C_{12}}{C_{21}} + \frac{C_{10}}{C_{01}}\right). \quad (\text{A14})$$

Thus from Equations A10 and A14 it is

$$\frac{n_1}{n_{\text{CI}}} = \frac{1}{1 + \frac{C_{12}}{C_{21}} + \frac{C_{10}}{C_{01}}} = \frac{g_1 e^{-E_1/kT_k}}{g_0 + g_1 e^{-E_1/kT_k} + g_2 e^{-E_2/kT_k}}, \quad (\text{A15})$$

which its expected LTE value. In the last derivations as well as in all previous computations we made use of the permutation relation  $C_{02}C_{21}C_{10} = C_{20}C_{01}C_{12}$  that results from the detailed balance equations.

In the radiation-dominated limit  $n_{10}/n \rightarrow \infty$  (and thus also  $n_{21}/n \rightarrow \infty$ ) we eventually deduce

$$\frac{n_1}{n_{\text{CI}}} \rightarrow \frac{g_1/g_0 f_{21} (f_{10} - 1)}{f_{21} [f_{10} + g_1/g_0 (f_{10} - 1)] + g_2/g_0 (f_{10} - 1) (f_{21} - 1)} = \frac{g_1 e^{-E_1/kT_b}}{g_0 + g_1 e^{-E_1/kT_b} + g_2 e^{-E_2/kT_b}}, \quad (\text{A16})$$

and

$$\frac{n_2}{n_1} \rightarrow \frac{g_2}{g_1} \left(\frac{f_{21} - 1}{f_{21}}\right) = \frac{g_2}{g_1} e^{-E_{21}/kT_b}, \quad \frac{n_1}{n_0} \rightarrow \frac{g_1}{g_0} \left(\frac{f_{10} - 1}{f_{10}}\right) = \frac{g_1}{g_0} e^{-E_{10}/kT_b}, \quad (\text{A17})$$

which are the values expected for levels fully regulated by the background radiation field.

The case where  $n_{21} \gg n_{10}$  allows partial thermalization of the 3-level system since there is a density domain where  $n_{10}/n \rightarrow 0$  while  $n_{21}/n$  remains finite and could be even  $\lesssim 1$ . We then find the limit

$$\frac{n_1}{n_0} \rightarrow \frac{g_1}{g_0} e^{-E_{10}/kT_k} \left\{ \frac{1 + \left(1 + \frac{C_{20}}{C_{21}}\right) \frac{C_{01}}{C_{02}} \left[1 + f_{21} \left(1 + \frac{C_{02}}{C_{01}}\right) \frac{n_{21}}{n}\right]}{1 + \left(1 + \frac{C_{20}}{C_{21}}\right) \frac{C_{01}}{C_{02}} \left[1 + f_{21} \left(1 + g_2/g_1 \left(\frac{f_{21}-1}{f_{21}}\right) \frac{C_{20}}{C_{10}} \frac{n_{21}}{n}\right)\right]} \right\}. \quad (\text{A18})$$

Interestingly this still deviates from its LTE value unless two more conditions are met, namely a)  $f_{21} \sim 1$  (negligible background at the  $\nu = \nu_{21}$  frequency), which yields

$$\frac{n_1}{n_0} \rightarrow \frac{g_1}{g_0} e^{-E_{10}/kT_k} \left\{ \frac{1 + \left(1 + \frac{C_{20}}{C_{21}}\right) \frac{C_{01}}{C_{02}} \left[1 + \left(1 + \frac{C_{02}}{C_{01}}\right) \frac{n_{21}}{n}\right]}{1 + \left(1 + \frac{C_{20}}{C_{21}}\right) \frac{C_{01}}{C_{02}} \left(1 + \frac{n_{21}}{n}\right)} \right\}, \quad (\text{A19})$$

and b)  $C_{02}/C_{01} \ll 1$  which then reduces the factor in the curly brackets to unity. These conditions ensure that the non-thermalized J=2 level has negligible interaction with the lower two either radiatively or collisionally. Condition (a) is usually satisfied for optically thin mm/sub-mm lines but condition (b) imposes a temperature constraint, namely

$$T_k \ll (E_{21}/k) \left[ \ln \left( \frac{g_2 C_{20}}{g_1 C_{10}} \right) \right]^{-1}. \quad (\text{A20})$$

In the case of the optically thin CI lines and since usually  $T_k \gg T_b \sim 2.7$  K we use the negligible radiation field approximation ( $f_{21} \sim f_{10} \sim 1$ ) to estimate the  $Q_{10}$  and  $Q_{21}$  factors, which are then are given by

$$Q_{10} = K^{-1} \left\{ 1 + \left( 1 + \frac{C_{20}}{C_{21}} \right) \frac{C_{01}}{C_{02}} \left[ 1 + \left( 1 + \frac{C_{02}}{C_{01}} \right) \frac{n_{21}}{n} \right] \right\}, \quad (\text{A21})$$

$$Q_{21} = K^{-1} \left[ \frac{C_{10}}{C_{20}} + \frac{C_{10} + C_{12}}{C_{21}} \left( 1 + \frac{n_{10}}{n} \right) \right]. \quad (\text{A22})$$

Using the detailed balance equations these become

$$Q_{10} = K^{-1} \left\{ 1 + \frac{g_1}{g_2} \left( 1 + \frac{C_{20}}{C_{21}} \right) \frac{C_{10}}{C_{20}} e^{E_{21}/kT_k} \left[ 1 + \left( 1 + \frac{g_2 C_{20}}{g_1 C_{10}} e^{-E_{21}/kT_k} \right) \frac{n_{21}}{n} \right] \right\} \quad (\text{A23})$$

$$Q_{21} = K^{-1} \left[ \frac{C_{10}}{C_{20}} + \left( \frac{C_{10}}{C_{21}} + \frac{g_2}{g_1} e^{-E_{21}/kT_k} \right) \left( 1 + \frac{n_{10}}{n} \right) \right]. \quad (\text{A24})$$

In the weak radiation field limit the expression for  $K$  becomes

$$K = 1 + \left( 1 + \frac{C_{20}}{C_{21}} \right) \left\{ \frac{n_{21}}{n} + \frac{C_{10}}{C_{02}} \left( 1 + \frac{C_{01}}{C_{10}} \right) \left[ 1 + \frac{C_{10}}{C_{01}} \left( \frac{1 + C_{12}/C_{10}}{1 + C_{10}/C_{01}} \right) \frac{n_{10}}{n} \right] \times \right. \\ \left. \left( 1 + \frac{n_{21}}{n} \right) \right\} + \frac{C_{12}}{C_{21}} \left( 1 + \frac{C_{10}}{C_{12}} \right) \left( 1 + \frac{n_{10}}{n} \right) + \frac{C_{10}}{C_{01}} \left( 1 + \frac{C_{01}}{C_{20}} \right), \quad (\text{A25})$$

or after some rearrangement of the terms and use of the detailed balance relations

$$K = 1 + \left( 1 + \frac{C_{20}}{C_{21}} \right) \left\{ \frac{n_{21}}{n} + \frac{g_0}{g_2} e^{E_2/kT_k} \left( 1 + \frac{g_1}{g_0} e^{-E_1/kT_k} \right) \frac{C_{10}}{C_{20}} G(n, T_k) \left( 1 + \frac{n_{21}}{n} \right) \right\} + \\ \frac{g_2}{g_1} e^{-E_{21}/kT_k} \left( 1 + \frac{g_1 C_{10}}{g_2 C_{21}} e^{E_{21}/kT_k} \right) \left( 1 + \frac{n_{10}}{n} \right) + \frac{g_0}{g_1} e^{E_1/kT_k} \left( 1 + \frac{g_1 C_{10}}{g_0 C_{20}} e^{-E_1/kT_k} \right), \quad (\text{A26})$$

where we have set

$$G(n, T_k) = 1 + \frac{g_0}{g_1} e^{E_1/kT_k} \left( \frac{1 + \frac{g_2 C_{21}}{g_1 C_{10}} e^{-E_{21}/kT_k}}{1 + \frac{g_0}{g_1} e^{E_1/kT_k}} \right) \frac{n_{10}}{n} \quad (\text{A27})$$

The CI  $J=1-0$ ,  $J=2-1$  hyperfine lines have degeneracy factors given by  $g_J = 2J + 1$ , and energy levels  $E_1/k = 23.6$  K,  $E_2/k = 62.4$  K. Their Einstein coefficients are  $A_{10} = 7.93 \times 10^{-8} \text{s}^{-1}$ ,  $A_{21} = 2.68 \times 10^{-7} \text{s}^{-1}$ ,  $A_{20} = 2 \times 10^{-14} \text{s}^{-1}$ , and their collisional rates  $\gamma_{10} = 1.3 \times 10^{-10} \text{cm}^3 \text{s}^{-1}$ ,  $\gamma_{21} = 7.8 \times 10^{-11} \text{cm}^3 \text{s}^{-1}$ ,  $\gamma_{20} = 2.0 \times 10^{-10} \text{cm}^3 \text{s}^{-1}$  with a very weak temperature dependance (Zmuidzinas et al. 1988 and references therein). Thus the critical densities as defined previously are  $n_{21} = 964 \text{cm}^{-3}$  and  $n_{10} = A_{10}/(\gamma_{10} + \gamma_{12}) = n_{10}(0) \left[ 1 + (g_2/g_1) e^{-E_{21}/kT_k} \gamma_{21}/\gamma_{10} \right]^{-1}$ . The latter varies from  $\sim 600 \text{cm}^{-3}$  ( $T_k = 0$  K) to  $\sim 300 \text{cm}^{-3}$  (high temperature limit).

## REFERENCES

- Aalto S., Booth R. S., Black J. M., & Johansson L. E. B. 1995 *A&A*, 300, 369
- Arimoto N., Sofue Y., & Tsujimoto T., 1996, *PASJ*, 48, 275
- Barone L. T., Heithausen A., Huttemeister S., Fritz T., & Klein U., 2000, *MNRAS*, 317, 649
- Baker A. J., Tacconi L. J., Genzel R., Lehnert M. D., & Lutz D. 2003 in *The Neutral ISM in Galaxies*, Marstrand, Sweden, (in preparation)
- Barvainis R., Maloney P., Antonucci R., & Alloin D. 1997, *ApJ*, 484, 695
- Bash F. N., Green E., & Peters W. L. 1977, *ApJ*, 217, 464
- Bennett, C. L., et al. 1994, *ApJ*, 434, 587
- Blain A. W. 1999, *MNRAS*, 304, 669
- Blain A. W., Frayer D. T., Bock J. J., & Scoville N. Z. 2000, *MNRAS*, 313, 559
- Blitz L., & Shu F. H. 1980, *ApJ*, 238, 148
- Bolatto A. D., Jackson J. M., & Ingalls J. G. 1999, *ApJ*, 513, 275
- Bolatto A. D., Jackson J. M., Kraemer K. E., & Zhang X. 2000a, *ApJ*, 541, L17
- Bolatto A. D., Jackson J. M., Wilson C. D., & Moriarty-Schieven G. 2000b, *ApJ*, 532, 909
- Braine J., & Combes F., 1992, *A&A*, 264, 433
- Bryant P. M., & Scoville N. Z., 1996, *ApJ*, 457, 678
- Brown R. L., & vanden Bout P. A. 1991, *AJ*, 102, 1956
- Brown R. L., & Vanden Bout P. A., 1992, *ApJ*, 397, L11
- Carilli C. L., Menten K. M., & Yun M. S. 1999, *ApJ*, 521, L25
- Carilli C. L., Cox P., Omont A., Djorgovski S. G., Petric A., Beelen A., Isaak K. G., & McMahon R. G. 2002a, *ApJ*, 575, 145
- Carilli C. L. et al. 2002b, *AJ*, 123, 1838
- Carilli C. L., & Blain A. W. 2002c, *ApJ*, 569, 605
- Chapman S. C., Blain A. W., Ivison R. J., & Smail I. R. 2003, *Nature*, Vol. 422, pg. 695
- Chiar J. E., Kutner M. L., Verter F., & Leous J., 1994, *ApJ*, 431, 658
- des Forêts G. P., Roueff E., & Flower D. R. 1992, *MNRAS*, 258, 45
- de Boisanger C., & Chiéze J. P. 1991, *A&A*, 241, 581
- Devereux N., Taniguchi, Y., Sanders D. B., Nakai N., Young J. S., 1994, *AJ*, 107 (6), 2006
- Downes, D., Solomon, P. M. 1998, *ApJ*, 507, 615
- Downes D., Radford S. J. E., Greve A., Thum C., Solomon P. M., & Wink J. E. 1992, *ApJ*, 398, L25
- Dickman R. L., Snell R. L., & Schloerb F. P., 1986, *ApJ*, 309, 326
- Digel S., de Geus E., & Thaddeus P., 1994, 422, 92
- Ellis R. 2001, *PASP*, 113, 515
- Elmegreen B. G. 1989, *ApJ*, 338, 178
- Elmegreen B. G. 2002, *ApJ*, 577, 206
- Evans A. S., Frayer D. T., Surace J. A., & Sanders D. B. 2001, *AJ*, 121, 3285
- Falgarone E., Panis J.-F., Heithausen A., Stutzki J., Puget J.-L., & Bensch F. 1998, *A&A*, 331, 669
- Flower D. R., Le Bourlot J., des Forêts G. P., & Roueff E. 1994, *A&A*, 282, 225
- Frayer D. T., & Ivison R. J., Scoville N. Z., Evans A. S., Yun M. S., Smail I., Barger A. J., Blain A. W., & Kneib J.-P. 1999, *ApJ*, 514, L13
- Fixsen D. J., Bennett C. L., & Mather J. C. 1999, *ApJ*, 526, 207
- Genzel R., Baker A. J., Tacconi L. J., Lutz D., Cox P., Guilloteau S., & Omont A. 2003, *ApJ*, 584, 633
- Gerin M., & Phillips T. G., 2000, *ApJ*, 537, 644
- Greve T., Ivison R. J. I., & Papadopoulos P. P. 2003, *ApJ* (in press)
- Harrison A., Puxley P., Russel A., & Brand P. 1995, *MNRAS*, 277, 413

- Hasegawa T., 1997, in IAU Symposium No. 170, *CO: Twenty-five years of millimeter-wave spectroscopy*, p. 39 (Kluwer Academic Publishers)
- Tielens A. G. G. M., & Hollenbach D. 1985a, *ApJ*, 291, 722
- Tielens A. G. G. M., & Hollenbach D. 1985b, *ApJ*, 291, 747
- Hollenbach D. J., Takahashi T., & Tielens A. G. G. M., 1991, *ApJ*, 377, 192
- Hollenbach D. J., & Tielens A. G. G. M. 1999, *Reviews of Modern Physics*, Vol 71, No 1, 174
- Ikeda M., Oka T., Tatematsu K., Sekimoto Y., Yamamoto S. 2002, *ApJS*, 139, 467
- Israel F. P., 1988, in *Millimetre and Submillimetre Astronomy*, R. D. Wolstencroft and W. B. Burton eds. Kluwer Academic Publishers, p. 281
- Israel F. P., 1997, *A&A*, 328, 471
- Israel F. P., Tilanus R. P. J., & Baas F. 1998, *A&A*, 339, 398
- Israel F. P., & Baas F. 2002, *A&A*, 383, 82
- Ivison R. J., Papadopoulos P. P., Seaquist E. R., & Eales S. A. 1996, *MNRAS*, 278, 669
- Jansen D. 1995, PhD Thesis, Leiden Observatory
- Johansson L. E. B., Olofsson H., Hjalmarson A., Gredel R., & Black J. H. 1994, *A&A*, 291, 89
- Jura M. 1975, *ApJ*, 197, 575
- Kaufman M. J., Wolfire M. G., Hollenbach D. J., & Luhman M. L., 1999, *ApJ*, 527, 799
- Keene J., Blake G. A., Phillips T. G., Huggins P. J., & Beichman C. A. 1985, *ApJ*, 299, 967
- Keene J., Lis D. C., Phillips T. G., & Schilke P. 1997, in *Molecules in astrophysics: probes & processes* IAU Symposium No 178, ed. Ewine van Dishoeck (Cambridge: Cambridge Univ. Press) 129
- Langer W. D., & Penzias A. A. 1993, *ApJ*, 408, 539
- Lee H.-H., Herbst E., des Forêts G. P., Roueff E., & Le Bourlot J. 1996, *A&A*, 311, 690
- Le Bourlot J., des Forêts G. P., & Roueff E. 1993, *ApJ*, 416, L87
- Lioure A., & Chiéze J. P. 1990, *A&A*, 235, 379
- MacLow M.-M., Klessen R. S., Burkert A., & Smith M. D. 1998, *Phys. Rev. Lett.*, 80, 2754
- Madden S. C., Poglitsch A., Geis N., Stacey G. J., & Townes C. H. 1997, *ApJ*, 483, 200
- McCall B. J., et al. 2003, *Nature*, 422, 500
- Maloney P. M., & Black J. H., 1988, *ApJ*, 325, 389
- Mehlert D., et al. 2002, *A&A*, 393, 809
- Meixner M., & Tielens A. G. G. M. 1993, *ApJ*, 405, 216
- Nakai N., & Kuno N. 1995, *PASJ*, 47, 761
- Neri R., Genzel R., Ivison R. J., Bertoldi F., Blain A. W., Chapman S. C., Cox P., Greve T. R., Omont A., & Frayer D. T. 2003, *astro-ph/0307310*
- Ojha R., Stark A. A., Hsieh H. H., Lane A. P., Chamberlin R. A., Bania T. M., Bolatto A. D., Jackson J. M., & Wright G. A. 2001, *ApJ*, 548, 253
- Oka T., Hasegawa T., Handa T., Hayashi M., & Sakamoto S. 1996, *ApJ*, 460, 334
- Oka T., et al., 2001, *ApJ*, 558, 176
- Omont A., Petitjean P., Guilloteau S., McMahon R. G., Solomon P. M., & Pécontal E. 1996, *Nature*, Vol 382, 428
- Pak S., Jaffe D. T., van Dishoeck E. F., Johansson L. E. B., & Booth R. S. 1998, *ApJ*, 498, 735
- Papadopoulos P. P., & Seaquist E. R., 1998, *ApJ*, 492, 521
- Papadopoulos P. P., & Ivison R. J. I., 2002, *ApJ*, 564, L9
- Papadopoulos P. P. 2004 (in preparation).
- Parravano A., Hollenbach D. J., McKee C. F. 2003, *ApJ*, 584, 797
- Pettini M., Steidel C. C., Adelberger K. L., Dickinson M., & Giavalisco M. 2000, *ApJ*, 528, 96
- Petitpas G. R., & Wilson C. D. 1998, *ApJ*, 503, 219

- Phillips T. G., & Huggins P. J. 1981, ApJ, 251, 533
- Rickard L. J., & Blitz L., 1985, ApJ, 292, L57
- Sakamoto S., Hasegawa T., Handa T., Hayashi M., & Oka T., 1997, ApJ, 486, 276
- Sanders D. B., Scoville N. Z., & Soifer B. T. 1991, ApJ, 370, 158
- Sawada T., et al. 2001, ApJS, 136, 189
- Schilke P., Carlstrom J. E., Keene J., & Phillips T. G. 1993, ApJ, 417, L67
- Solomon P. M., Scoville N. Z., & Sanders D. B., 1979, ApJ, 232, L89
- Solomon P. M., Downes D., & Radford S. J. E. 1992, ApJ, 398, L29
- Solomon P. M., Downes D., Radford S. J. E., & Barrett J. W. 1997 ApJ, 478, 144
- Somerville R. S., Primack J. R., Faber S. M. 2001, MNRAS, 320, 504
- Spaans M., & van Dishoeck E. F., 1997, A&A, 323, 953
- Stark A. A., Bolatto A. D., Chamberlin R. A., Lane A. P., Bania T. M., Jackson J. M., & Lo K.-Y. 1997, ApJ, 480, L59
- Steidel C. C., Giavalisco M., Pettini M., Dickinson M., & Adelberger K. L. 1996, ApJ, 462, L17
- Stone J. M., Ostriker E. C., & Gammie C. F. 1998, ApJ, 508, L99
- Störzer, H., Stutzki J., & Sternberg A. 1997, A&A, 323, L13
- Stutzki J., et al. 1997, ApJ, 477, L33
- Suchkov A., Allen R. J., & Heckman T. M., 1993, ApJ, 413, 542
- Tauber J. A. 1996, A&A, 315, 591
- van Dishoeck et al. 1992, in IAU Symposium *Astrochemistry of Cosmic Phenomena*, P. D. Singh (ed.) pg 285
- Weiss A., Henkel C., Downes D., & Walter F. 2003, A&A, 409, L41
- Wilson C. D. 1997, ApJ, 487, L49
- Wilson C. D., Howe J. E., & Balogh M. L., 1999, ApJ, 517, 174
- White G. J., Ellison B., Claude S., Dent W. R. F., & Matheson D. N. 1994, A&A, 284, L23
- Wolfire M. G., McKee C. F., Hollenbach D., & Tielens A. G. G. M. 2003, ApJ, 587, 278
- Xie T., Allen M., & Langer W. D. 1995, ApJ, 440, 674
- Xie T. 1997, in *CO: Twenty-five years of millimeter-wave spectroscopy*, IAU Symposium No 170, W. B. Latter et al. (eds.) (Kluwer Academic Publishers) p. 131
- Yamamoto et al. 2001, ApJ, 547, L165
- Young J. S., & Scoville N. Z. S., 1991, ARAAS, Vol 29, 581
- Zhang X., Lee Y., Bolatto A., & Stark A. A. 2001, ApJ, 553, 274
- Zmuidzinas J., Betz A. L., Boreiko R. T., & Goldhaber D. M. 1998, ApJ, 335, 785